DOE/JPL-954877-78/3
Dist. Category UC-63

STUDY PROGRAM TO DEVELOP AND EVALUATE DIE AND CONTAINER MATERIALS FOR THE GROWTH OF SILICON RIBBONS

Paul E. Grayson, Program Manager
Larry A. Addington, Project Engineer

Miami Research Laboratories
Eagle-Picher Industries, Inc.
Miami, Oklahoma 74354

QUARTERLY REPORT NO. 4

OCTOBER 1978

The JPL Low-Cost Silicon Solar Array Project is funded by DOE and forms part of the DOE Photovoltaic Conversion Program to initiate a major effort toward the development of low-cost solar arrays.

Prepared Under Contract No. 954877 for
JET PROPULSION LABORATORY
CALIFORNIA INSTITUTE OF TECHNOLOGY
Pasadena, California 91103

EAGLE EP PICHER

DOE/JPL-954877-78/3
Dist. Category UC-63

STUDY PROGRAM TO DEVELOP AND EVALUATE DIE AND CONTAINER MATERIALS FOR THE GROWTH OF SILICON RIBBONS

Paul E. Grayson, Program Manager
Larry A. Addington, Project Engineer

Miami Research Laboratories
Eagle-Picher Industries, Inc.
Miami, Oklahoma 74354

QUARTERLY REPORT NO. 4

OCTOBER 1978

The JPL Low-Cost Silicon Solar Array Project is funded by DOE and forms part of the DOE Photovoltaic Conversion Program to initiate a major effort toward the development of low-cost solar arrays.

Prepared Under Contract No. 954877 for
JET PROPULSION LABORATORY
CALIFORNIA INSTITUTE OF TECHNOLOGY
Pasadena, California 91103

EAGLE PICHER

ACKNOWLEDGEMENT

This report represents the combined work of Paul Grayson, (MRL); Larry Addington, (MRL); Dr. P.D. Ownby, (UMR); Dr. Bu-Fan Yu, (UMR); Mike Barsoum, (UMR); and Brian Zealear (Chemetal). The support of George Alexander (MRL) in x-ray and SEM characterization is acknowledged. Special mention is due Gene Cantwell (MRL) and Dr. Jim Thomas (Pittsburg State University, Kansas) for the detailed investigation of the x-ray peculiarities of the CNTD coatings.

The cheerful assistance of Ms. Mary Holland and Mr. Ginn in typing and organizing the many drafts of the various inputs is also deeply appreciated.

SUMMARY

Die and container material development efforts under the current program are shared among three organizations. Miami Research Laboratories (MRL) - ceramic process development and overall program management, University of Missouri - Rolla (UMR) - silicon sessile drop studies with characterization of reaction products and emphasis on atmospheric effects, Chemetal Corporation, Pacoima, California - special coatings to be applied to test coupons, die shapes and containers provided by MRL and tested/characterized by UMR.

Initial sessile drop experiments on SiC, Si_3N_4 and AlN have been conducted. Very promising results have been achieved on both SiC and Si_3N_4 where minimal penetration of these CNTD coatings by molten silicon was observed.

Efforts during the past quarter continued in the following areas. At MRL more detailed characterization of the CNTD microstructures was accomplished as well as x-ray characterization of the third and fourth candidate materials system sets (ie. AlN and altered Si_3N_4). Polished sections of post sessile drop specimens were also prepared and evaluated. The results of the latter continue to be encouraging. The techniques of full scale crucible hot pressing were developed and die grinding development was initiated.

At UMR the apparatus for measurement of oxygen partial pressure was reconstructed and calibrated with a known reference gas to overcome flow rate effects. The sessile drop temperature measurement procedure was calibrated for absorption by the pyrex view-port and additional Auger electron analysis was performed at the interface of molten silicon with CNTD Si_3N_4 and AlN.

At Chemetal production of altered Si_3N_4 coatings on hot pressed discs for UMR sessile drop experiments was completed.

TABLE OF CONTENTS

Section			Page
	ACKNOWLEDGEMENT		i
	SUMMARY		ii
	TABLE OF CONTENTS		iii
	LIST OF TABLES		v
	LIST OF FIGURES		vi
1.	INTRODUCTION		1
	1.1	PROGRAM GOALS	1
	1.2	MATERIALS UNDER INVESTIGATION	1
2.	MIAMI RESEARCH LABORATORY EFFORTS		3
	2.1	MICROSTRUCTURAL CHARACTERIZATION OF FIRST AND SECOND CANDIDATE MATERIALS SETS	3
		2.1.1 First Candidate Materials Set-SiC	3
		2.1.2 Second Candidate Material Set - Si_3N_4	9
	2.2	CHARACTERIZATION OF THIRD CANDIDATE MATERIALS SET-AlN	12
	2.3	CHARACTERIZATION OF FOURTH CANDIDATE MATERIALS SET - ALTERED Si_3N_4	16
		2.3.1 X-Ray Diffraction Analysis	16
		2.3.2 Microstructure	19
	2.4	CHARACTERIZATION AFTER SESSILE DROP EXPERIMENTS	25
		2.4.1 First Candidate Materials Set - SiC	25
		2.4.2 Second Candidate Materials Set - Si_3N_4	27
		2.4.3 Third Candidate Materials Set - AlN	31
	2.5	DIE AND CRUCIBLE FABRICATION	31

Table of Contents - continued

Section			Page
3.	UMR EFFORTS		35
	3.1	MEASUREMENT OF OXYGEN PARTIAL PRESSURE	35
		3.1.1 ThO_2 - 7wt% Y_2O_3 Solid Electrolyte Cell	36
		3.1.2 Method to Overcome the Flow Rate Effects	39
		3.1.3 A Known P_{O_2} Atmosphere Source-CO/CO_2 Buffering System	39
		3.1.4 Calibration and Development of the Oxide Cell	41
	3.2	TEMPERATURE CALIBRATION	41
	3.3	SESSILE DROP EXPERIMENTS	45
	3.4	CHARACTERIZATION	48
4.	CHEMETAL EFFORTS		65
5.	CONCLUSIONS		65
6.	PROJECTED ACTIVITIES FOR THE FIFTH QUARTER		66
	6.1	MIAMI RESEARCH LABORATORIES	66
	6.2	UNIVERSITY OF MISSOURI - ROLLA	67
	6.3	CHEMETAL	67
	REFERENCES		68
	APPENDIX - DETAILED DISCUSSION OF THE X-RAY DIFFRACTION CHARACTERIZATION OF THE ALTERED Si_3N_4 COATINGS (GROUP 4-A & 4-B)		69
	A.1	PEAK IDENTIFICATION	A-1
	A.2	RELATIVE INTENSITES	A-2

LIST OF TABLES

Table		Page
I	Spectrographic Analysis of AlN Powder, ESK Lot No. 312872	13
II	Chemetal Observations and X-Ray Diffraction Results, CNTD AlN Coatings on Hot Pressed AlN	15
III	Chemetal Observations and X-Ray Diffraction Results, Altered Si_3N_4 Deposited on Hot Pressed Si_3N_4 w/10wt% Y_2O_3, Materials Candidate Set 4-A, Si_2ON_2 Attempt	17
IV	Chemetal Observations and X-Ray Diffraction Results, Altered Si_3N_4 Deposited on Hot pressed Si_3N_4 w/10wt% Y_2O_3, Materials Candidate Set 4-B, SiAlON Attempt	18
V	Galvanic EMF Output From the ThO_2 - 7 wt% Y_2O_3 Solid-Electrolyte Cell for Various Oxygen-Partial-Pressure Atmospheres	42
VI	Brightness Temperature[1] (at wave length 0.65 microns) as a Function of Lamp Current for Model No. 107 Calibration Set	44
VII	Calibration of Pyrometers' Reading to Reference Lamp Filament Temperature	46
VIII	Correction of the Pyrex Viewport Absorption at Various Temperatures	47
A-I	Calculated & Experimental Intensities	A-4
A-II	Ratios of (222) Peak Intensities to Five Strong Peaks[a]	A-7

LIST OF FIGURES

Figures		Page
1.	CNTD SiC Coating on Hot Pressed SiC	5
2.	Fractures Surface of CNTD SiC Coating on Hot Pressed SiC	5
3.	Polished and Electrochemically Etched Cross Section of CNTD SiC	6
4.	Polished and Thermally Etched Cross Section of CNTD SiC on Hot Pressed SiC	7
5.	SEM and EDX Investigation of Thermal Etching Details in CNTD SiC Coating	8
6.	Further SEM Investigation of Details of CNTD SiC Coating Microstructure	10
7.	Fractured Surface of CNTD Si_3N_4 Coating on Hot Pressed Si_3N_4 w/4 wt% MgO	11
8.	Candidate Materials Set 4-A at Low Magnification	20
9.	Scanning Electron Photomicrograph of Candidate Materials Set 4-B Coating known to contain both Crystalline and Amorphous Characteristics	22
10.	Optical Photomicrograph of Candidate Materials Set 4-B Coating Known to Contain Both Crystalline and Amorphous Characteristics	23
11.	SEM Photomicrographs of Candidate Materials Set 4-B Coating, Fractured Surface	24
12.	Polished and Etched Cross Section of Silicon Sessile Drop for Interface Investigation	26
13.	Post Sessile Drop Conditions for CNTD Si_3N_4 on "Impure", PP-30, Si_3N_4 Substrate	28
14.	Post Sessile Drop Conditions for CNTD Si_3N_4 on "Pure", PP-33, Si_3N_4 Substrate	29
15.	The Effects of a Crack in the CNTD Coating	30
16.	Polished Section of Interface Between Silicon Sessile Drop and CNTD AlN on Hot Pressed AlN Substrate	32
17.	Ionic Transference Numbers in Pure Thoria and Thoria Base Solid Solution with Yttria as a Function of Oxygen Partial Pressure at 1000°C	37

LIST OF FIGURES - continued

Figure		Page
18.	Apparatus for P_{O_2} Measurement	38
19.	Effect of Reference Gas Flow Rate on Galvanic EMF Output from the Cell at a Fixed CO/CO_2 gas Flow Rate	40
20.	Relationship Between Log P_{O_2} and Galvanic EMF Output at 1000° and 1100°C.	43
21.	Silicon Penetration of a Crack in a CNTD Si_3N_4 Coating	49
22.	Post Sessile Drop Auger Electron Surface Analysis CNTD Si_3N_4	51
23.	Variation of Carbon and Nitrogen dN/dE Auger Peaks with Time of Sputtering for Silicon on CNTD Si_3N_4	58
24.	Post Sessile Drop Auger Electron Surface Analysis, CNTD AlN	59
25.	Auger Electron Analysis of Silicon Drop Melted on CNTD AlN	62
A-8	Laue Camera Experimental Set-up for Investigating Possible Orientation in the Coatings	A-9

1. INTRODUCTION

The current program is a cooperative effort among three facilities to attack the die and container materials problems of the Low Cost Silicon Array Project. Miami Research Laboratories (MRL) provides overall project management as well as die and container fabrication engineering and characterization. Chemetal Corporation (Pacoima, California) applies ceramic coatings to substrates for testing and later to die and container shapes made by MRL using the proprietary "CNTD" (Controlled Nucleation by Thermochemical Decomposition) process. University of Missouri-Rolla (UMR) personnel perform sessile drop experiments on coated substrates made by MRL and Chemetal. They are investigating the effects of oxygen partial pressure and characterizing the reactions using Auger spectroscopy, ESCA and other techniques.

1.1 PROGRAM GOALS

The goals of the present program are to develop successful die and container materials for handling liquid silicon while it is being formed into photovoltaic cell material. These goals will be accomplished by exploring various material configurations for their reactivity with molten silicon. The combination of unique coating structures combined with control of oxygen partial pressures may yield a set of conditions which are useful for cost effective dies and/or containers for pulling ribbons from silicon melts. Successful experimental configurations will be scaled up into prototype dies and containers as appropriate during the third and fourth quarters of calendar 1978. Economics for large scale production of such prototypes will be defined as part of the program.

1.2 MATERIALS UNDER INVESTIGATION

Silicon sessile drop specimens of the following candidate material configurations have been fabricated by MRL and coated by Chemetal

to be tested for contact angle and reactivity at UMR. The first candidate system is CNTD SiC coatings on hot pressed discs (dimensions 1.2" dia. x 0.165" thick) of SiC w/1wt%B as a densification aid. The second candidate materials system consists of pure CNTD Si_3N_4 coatings on two types of hot pressed Si_3N_4 discs - an "impure" (95-98% Si_3N_4) and a "pure" (99.9%), both with 4wt% MgO added as a densification aid. The third candidate materials system consists of CNTD AlN coatings on hot pressed AlN discs (powder pressed as received). The fourth candidate materials system was produced in a development effort aimed at depositing an altered form of CNTD Si_3N_4 on hot pressed discs of Si_3N_4 (97-98% pure) with 10wt% Y_2O_3 added as a densification aid. These coatings were deposited by the proprietary Chemetal process but with the introduction of oxygen and/or aluminum bearing gases during the deposition process. Two types of altered Si_3N_4 structures were taken under development. The first (4-A) was an attempt to introduce oxygen into the Si_3N_4 crystal lattice and form Si_2ON_2. The second was an attempt to introduce oxygen and aluminum into the lattice and form Si_3N_4 polymorphs in the SiAlON system.

X-ray diffraction phase identification of the coatings in the first and second materials systems was given in the third quarterly report of this program. Phase identification of the third and fourth materials systems are provided in this report (see sections 2.2 and 2.3 respectively).

2. MIAMI RESEARCH LABORATORY EFFORTS

MRL activities this period included the continued investigation of the microstructure of CNTD SiC and Si_3N_4 to compliment the previously reported x-ray diffraction data as well as the general characterization of the third (AlN) and fourth (altered Si_3N_4) candidate materials sets. The fourth set general characterization includes both microstructural and x-ray diffraction data.

More extensive characterization of the results of the sessile drop runs reported in the previous quarter's work has been completed. The emphasis at MRL has been on optical microscopy while that of UMR has been on Auger Spectroscopy (see section 3.4).

The fabrication of die and crucible shapes for coating by Chemetal has been pursued at MRL in addition to the characterization work. The first die and crucible delivery requirement was elected to be fulfilled with the Si_3N_4 materials system. This system was chosen for first delivery in lieu of SiC because of raw materials and tooling availability and the anticipation of a less extensive hot pressing development requirement.

2.1 MICROSTRUCTURAL CHARACTERIZATION OF FIRST AND SECOND CANDIDATE MATERIALS SETS

2.1.1 First Candidate Materials Set - SiC

The Chemetal CNTD process has demonstrated the capability of producing fine grained, high density materials, however, there is an apparent tendency to form a relatively coarse "macrostructure" the elements of which exhibit extremely fine grained microstructure. The elements of the "macrostructure" may not be "grains" as the term is applied to conventional ceramic materials, and their appearance is dependent upon the methods used in investigating them. Figure 1 shows the as-

deposited surface to appear nodular, but, with indications of a finer substructure. Figure 2 shows a fractured surface of the same specimen with an apparent columnar structure in the coating, parallel with the direction of growth. Careful examination of the photograph reveals fine relief on the larger, relatively smooth surfaces.

This same specimen was diamond polished and electrolytically etched in an aqueous solution of 5 wt% CrO_3 and 1 wt% HF. The results of this treatment is shown in Figure 3. The etching of the specimen in Figure 3 is very light and has not provided any elucidation of the hot pressed substrate grain structure. The CNTD coating "macrostructure" exhibits variations of color within and between the individual regions, ranging from blue to red for light etching. After longer periods of etching the coloring and macrostructural appearance are lost.

The electrolytic etch did not appear to reveal the ultimate crystallite size contained in these coatings, and for this reason thermal etching was investigated. Figure 4 represents the etch pattern developed after etching in a graphite muffle with flowing argon for 1 hour at 1400^{o}C. The pattern which developed is much different than that revealed by electrolytic etching in Figure 3. It may be noted that the thermal etch was much more effective than the electrochemical etch in elucidating the microstructure of the hot pressed substrate. Figure 4-b shows that finer texturing of the CNTD material exists.

The apparent bright spots in the optical photomicrographs were further investigated using the SEM in the EDX mode. The coatings were found to be free of metallic impurities and a silicon map across an area containing these patterns revealed no substantial variations in silicon content related to these features, (see Figure 5).

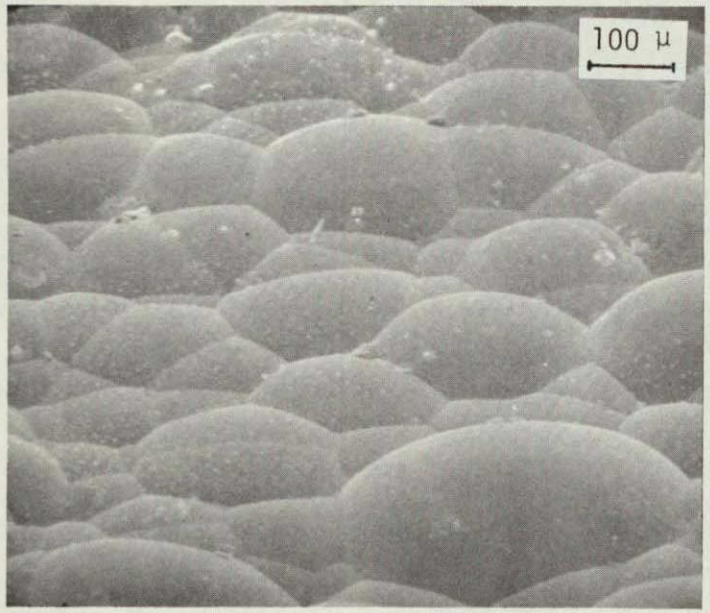

Figure 1. CNTD SiC Coating on Hot Pressed SiC

Lot PP-26, Part No. 9 as deposited, 118X indicates fine grain sub-structure, SEM.

Coating ↓

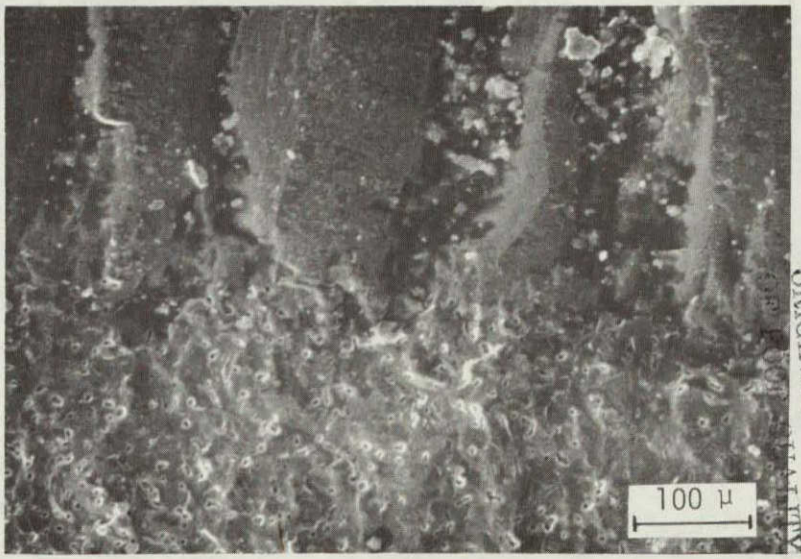

Hot Pressed Substrate ↑

Figure 2. Fractured Surface of CNTD SiC Coating on Hot Pressed SiC

Lot PP-26, Part No. 9, 160X, regions of finer structure between apparent columns, SEM.

Coating ↓

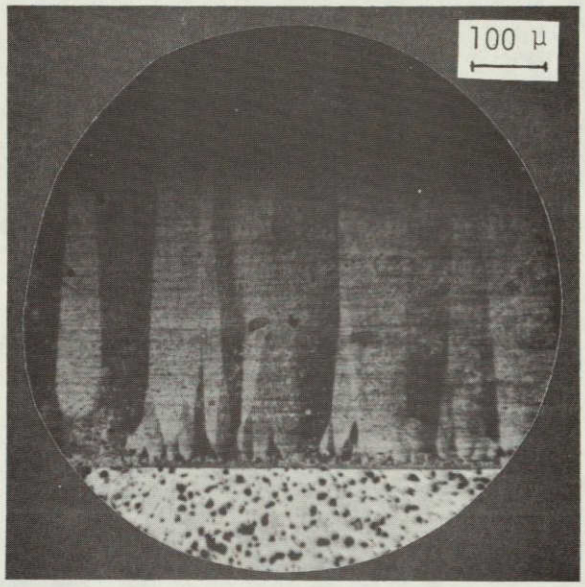

Hot Pressed Substrate ↑

Figure 3. Polished and Electrochemically Etched Cross Section of CNTD SiC Lot PP-26, Part No. 9, 100X, Optical.

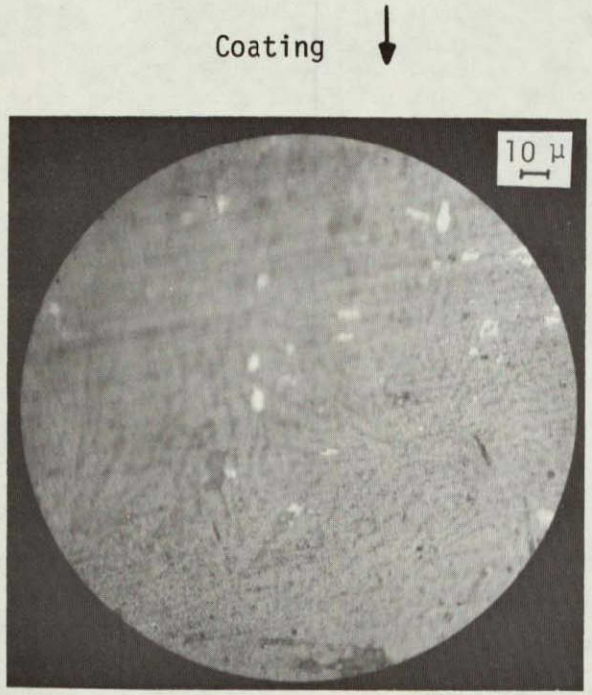

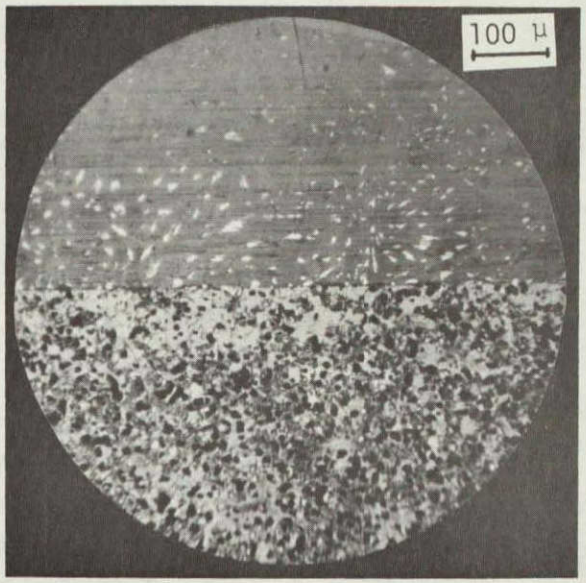

a) - 100X

b) - 400X

Figure 4. Polished and Thermally Etched Cross Section of CNTD SiC on Hot Pressed SiC

Lot PP-26, Part No. 9, etched in graphite muffle with flowing argon for 1 hr. at 1400°C, optical photomicrographs

a)

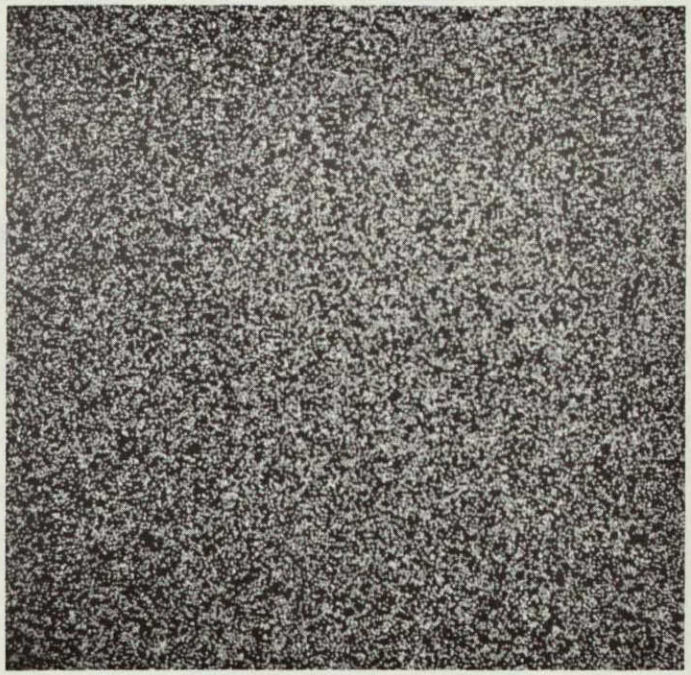

b)

Figure 5. SEM and EDX Investigation of Thermal Etching Details in CNTD SiC Coating

Lot PP-26, Part No. 9, etched in graphite muffle with flowing argon for 1 hour, at 1400°C

a) SEM at 1200X
b) Silicon map of identical area as shown in Figure 5-a

The thermal etch was not uniform in its action on the CNTD coating. This is shown in Figure 6-a. Silicon maps were made and no substantial variation in silicon content was noted from one region to another. The greatest achievement to date in revealing the grain size potential for CNTD fabrication in this program is shown in Figure 6-b. Grains as small as 0.25 μ (2500 Å) are revealed. While this microstructure has not been shown to be representative of all regions, or all samples, the potential of CNTD fabrication for production of dense, fine grained, SiC coatings is thus demonstrated.

2.1.2 Second Candidate Materials Set - Si_3N_4

The microstructural information obtained for the CNTD Si_3N_4 coatings has been observed on fractured specimens. These coatings appear extremely dense. Figure 7-a shows the CNTD structure at 2000X and suggests a grain size on the order of 20 to 25 μ. A larger magnification (Figure 7-b) reveals grains on the order of 1 μ or less, demonstrating the capability of CNTD fabrication to produce reasonably fine grained Si_3N_4.

Polished sections have been prepared, however, a chemical or electrochemical etch capable of even moderate elucidation of the microstructure was not found. The examination of past sessile drop coatings in the SEM from a perspective perpendicular to the coated surface in an area adjacent to but not including the silicon drop has shown some microstructural details. The semi-fine lapping which was performed on the deposited surface to facilitate sessile drop experiments was apparently adequate for the sessile drop runs to provide thermal etching. This will allow more efficient evaluation of CNTD microstructures.

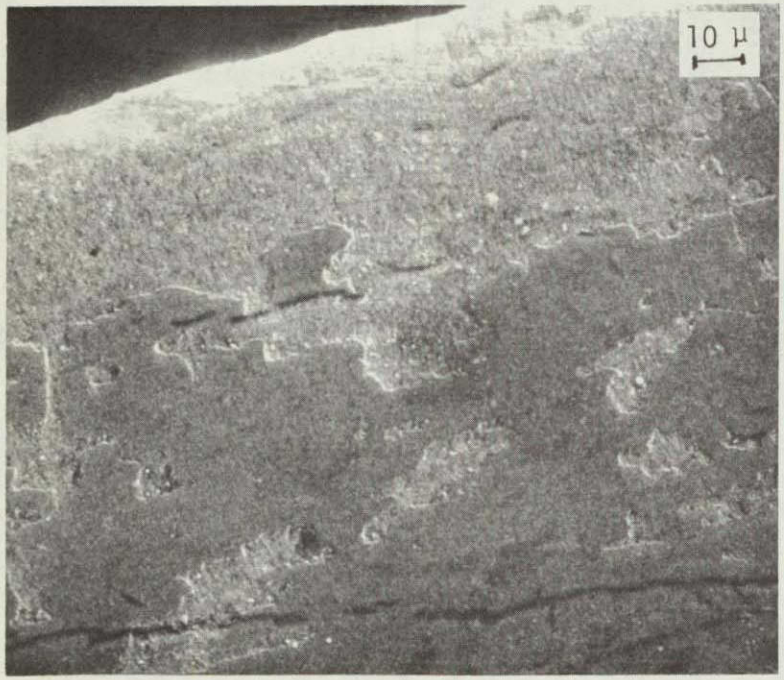

a)

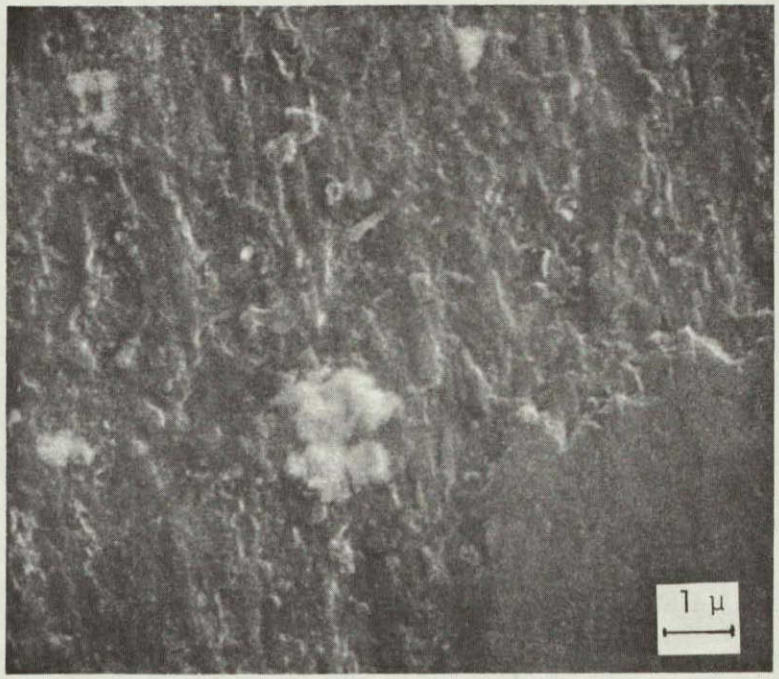

b)

Figure 6. Further SEM Investigation of Details of CNTD SiC Coating Microstructure

a) Nonuniform etching, 600X
b) Resolution of fine grained region, 9000X

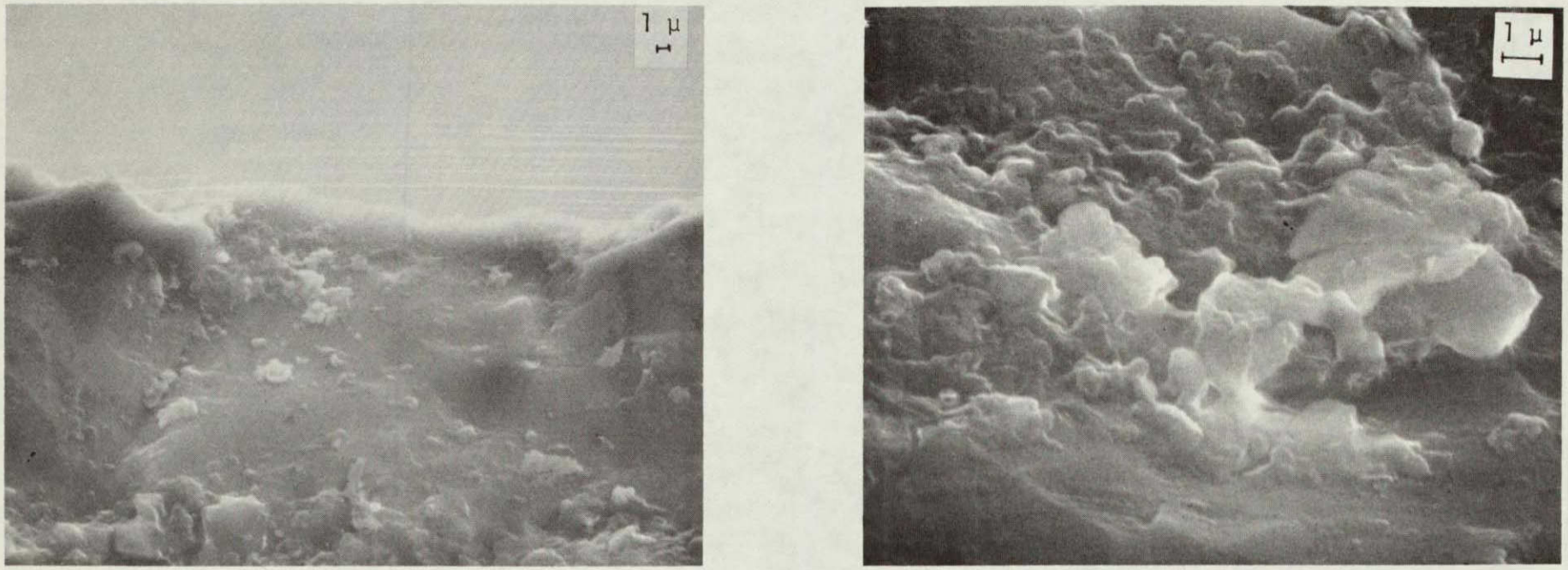

a) - 2000X

b) - 6000X

Figure 7. Fractured Surface of CNTD Si_3N_4 Coating on Hot Pressed Si_3N_4 w/4 wt% MgO.

Lot PP-33, Part No. 3, showing variances in texture from moderate to extremely fine grained, all coating

TABLE I.

Spectrographic Analysis of AlN Powder, ESK Lot No. 312872

IMPURITY	ANALYSIS[1] (PPM)
B	100
Mn	50
Pb	5
Mg	50
Si	500
Fe	10,000[2]
Al	major
Cu	20
Ni	10
Ca	20
Cr	40

1. Semiquantitative Estimation by emission spectrograph, Sample CG7807AV

2. A second sample CG7808BG was analysed and results were 7,300 PPM Fe.

up to three of the eight suspect positions indicating there was some tendency for the impurity (ies) to "bleed through".

The relative peak heights observed in the patterns obtained from the CNTD AlN coatings were not in the same ratios as those given in the ASTM card file, although the peak positions were correct. This is not surprising for a CVD type coating, and has been attributed, by the author, to orientation effects, or structure factor changes.

The 100 peak was consistently low and the 101, 102, 103, 112, and 203 peaks were consistently high. The orientation of the deposited crystallites and/or other factors effecting peak height are thus assumed to be consistent from specimen to specimen.

A summary of the Chemetal observations and MRL x-ray diffraction results are shown in TABLE II.

TABLE II

Chemetal Observations and X-Ray Diffraction Results, CNTD AlN Coatings on Hot Pressed AlN

Chemetal Designation	MRL Designation	Coating Thickness	Chemetal Observations	MRL X-Ray Diffrac. Results Morphology/Phases Present
1-4323-06-098	Part No. 1 of 30	0.0038"	Even deposit of medium size crystals, greenish color.	Hexagonal AlN, three unknown weak peaks, 102 and 103 peaks considerably higher than expected.
1-4323-07-098	Part No. 2 of 30	0.0228"	Black, even deposit of large crystals	As above
1-4323-08-098	Part No. 3 of 30	0.0072"	Even deposit of small crystals, reddish brown color.	As above
1-4323-09-098	Part No. 4 of 30	0.0063"	Small crystals, brown at center and green at edges.	As above
1-4323-10-098	Part No. 5 of 30	0.0062"	Very fine grain, small crystals, evenly deposited	As above
1-4323-11-098	Part No. 6 of 30	0.0146"	Medium size crystals with reddish-green color.	As above
1-4323-12-098	Part No. 7 of 30	0.0157"	Even deposit, medium size crystals.	As above, orientation effects quite strong.
1-4323-13-098	Part No. 8 of 30	0.0070"	Larger crystals than run 12, but still good.	As above, no unknown peaks.
1-4323-14-098	Part No. 9 of 30	0.0122"	Same as run 13.	As above
1-4323-16-098	Part No. 11 of 30	0.0086"	Small crystals, evenly deposited. Deposit cracked	As above, two unknown peaks
1-4323-17-098	Part No. 12 of 30	0.0112"	Small crystals, evenly deposited, good deposit.	One unknown peak, orientation effects strongest of all samples
1-4323-18-098	Part No. 13 of 30	0.0101"	Small crystals, similar to run 17.	Two unknown peaks, very strong orientation effects.

2.3 CHARACTERIZATION OF FOURTH CANDIDATE MATERIALS SET - ALTERED Si_3N_4

2.3.1 X-Ray Diffraction Analysis

The x-ray diffraction characterization of a thin coating, particularly one deposited from the vapor phase, is a complicated task and the CNTD materials proved to be no exception. The group 4-A and 4-B, altered Si_3N_4, coatings were given special attention owing to the complexity of the x-ray diffraction patterns one would expect to obtain from materials containing Si_2ON_2 and SiAlON respectively. The Chemetal observations and MRL x-ray diffraction results are given in Tables III and IV and show that the hopes of depositing Si_2ON_2 (4-A) and SiAlON (4-B) were not realized. Differences were observed, however, in the deposited condition and in the color when compared to the previously reported CNTD Si_3N_4 materials of the second candidate materials set. These materials may, therefore, behave differently in contact with molten silicon by virtue of stoichiometric or other considerations.

These coatings were analyzed on the diffractometer at two settings of the detector sensitivity, without demounting the specimen to facilitate relative intensity comparisons for peaks of widely varying height. The determination of phases present was relatively straight forward. The major complication was a slight angular shift of peak position which was determined by analysis of the same coatings on another machine to be due to mechanical problems related to the sample holder.

The analysis of relative intensities was considerably more difficult. Variations from the expected powder diffraction valves of up to 1000% were observed. The detailed discussion of these results

TABLE III

Chemetal Observations and X-Ray Diffraction Results, Altered Si_3N_4 Deposited on Hot Pressed Si_3N_4 w/10wt% Y_2O_3, Materials Candidate Set 4-A, Si_2ON_2 Attempt.

Chemetal Designation	MRL Designation	Coating Thickness	Chemetal Observations	MRL X-Ray Diffraction Results
1-4323-43-098	PP-40, Part No. 1 of 10	0.0032"	Deposit was amorphous with very fine cracks	Amorphous, no peaks
1-4323-44-098	Part 2 of 10	0.0071"	Fine crystals in Center, 1/8" O.D. rim amorphous	α-Si_3N_4
1-4323-45-098	Part 3 of 10	0.0066"	Deposit very similar to run #44, but larger crystals	α-Si_3N_4
1-4323-46-098	Part 4 of 10	0.0061"	Very fine crystals in center area with amorphous at outer diameter	α-Si_3N_4
1-4323-47-098	Part 5 of 10	0.0061"	Same as run #44	α-Si_3N_4
1-4323-48-098	Part 6 of 10	0.0061"	Crystalline deposit, smaller crystals in center	α-Si_3N_4
1-4323-51-098	Part 9 of 10	0.0058"	Similar to run #48	α-Si_3N_4; possible amorphous phase present

TABLE IV

Chemetal Observations and X-Ray Diffraction Results, Altered Si_3N_4 Deposited on Hot pressed Si_3N_4 w/10wt% Y_2O_3*, Materials Candidate Set 4-B, SiAlON Attempt

1-4323-49-098	PP-40, Part No. 7 of 10	0.0057"	Amorphous with fine cracks	Amorphous, no peaks
1-4323-50-098	Part 8 of 10	0.0042"	Same as run 49	" " "
1-4323-52-098	Part 10 of 10	0.0053"	Amorphous with network cracks	" " "
1-4323-54-098	*AlN Substrate Part No. 374-A	0.0142"	Center contained crystals. Outer diameter was bumpy.	α-Si_3N_4
1-4323-62-098	PP-40, Part No. 381-A	0.0139"	Large black crystals in center, very large black nodules on outside.	α-Si_3N_4
1-4323-65-098	Part 384-A	0.0127"	Amorphous deposit with crystalline nodules	α-Si_3N_4, possible amorphous phase present
1-4323-67-098	Part 381-B	0.0141"	Fine crystals at center with larger crystalline nodules near O.D.	α-Si_3N_4
1-4323-68-098	Part 383-A	0.0104"	Amorphous deposit with crystalline nodules	α-Si_3N_4
1-4323-69-098	Part 383-B	0.0105"	About 1/8" near O.D. crystalline with center amorphous with a few larger crystalline nodules.	α-Si_3N_4, possible amorphous phase present
1-4323-70-098	Part 386-A	0.0129"	All fine crystals	α-Si_3N_4
1-4323-71-098	Part 386-B	0.0144"	All fine crystals	α-Si_3N_4

are found in the Appendix. These intensity variations could be explained by an oriented growth pattern, a non-uniformity of crystallite size or a change in the structure factor due to the thermochemical mechanism of deposition, or nonstoichiometry or any combination of these.

The work done at MRL and at Pittsburg State University, Pittsburg, Kansas, (see Appendix) indicates that while preferred orientation cannot be ruled out, it did not exist in strong degree. The most probable explanation of the intensity variations is structure factor changes related to the thermochemical mechanism of deposition and/or nonstoichiometry.

The Laue back reflection experiments described in the Appendix did indicate that the coating contained crystallites in the range of 0.1 mm to 0.6 mm (100 to 600 μ). The scanning electron microscopic studies confirmed that a wide distribution of grain sizes existed in these coatings (see section 2.3.2).

2.3.2 Microstructure

The candidate materials set 4-A exhibited a relatively coarse crystalline appearance before grinding as shown in the optical photomicrograph in Figure 8-a. The typical appearance after grinding is illustrated in Figure 8-b. The coatings were translucent with the coloration observed to vary from faint grey to faint tan or a deeper brown from sample to sample but were reasonable uniform across a given sample.

They exhibited the network type cracks similar to those found in the CNTD Si_3N_4 of the second candidate materials set. Most of the cracks appeared to terminate within the coating rather than coming through to the polished surface.

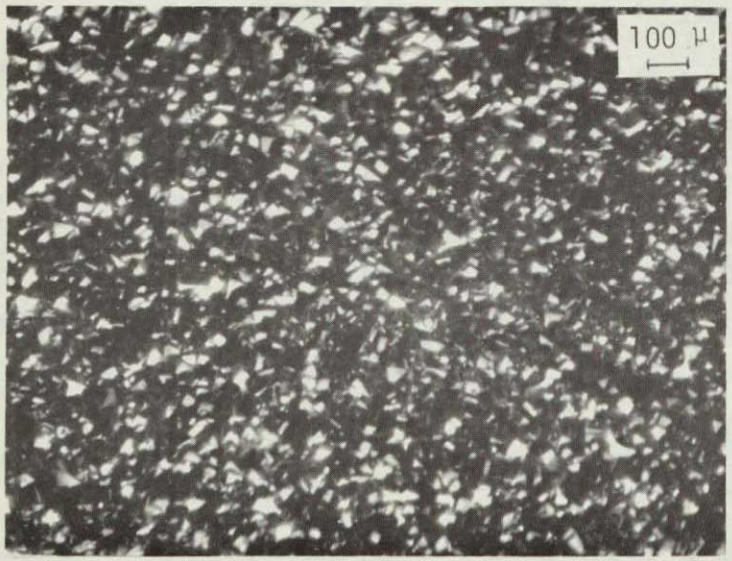

a)

b)

Figure 8. Candidate Materials Set 4-A at Low Magnification

a) PP-40, Part No. 2 of 10, as deposited, 52.5X
b) PP-40, Part No. 5 of 10, polished, 52.5X

The candidate materials set 4-B coatings also appeared coarsely crystalline as deposited. Figure 9 is a scanning electron photomicrograph of a coating shown by x-ray diffraction to be partly crystalline and partly amorphous. The crystalline region is readily apparent. The botryoidal regions may contain the amorphous phase although this was not verified. The specimen was also examined by EDX analysis to check for Al which might be contained in the lattice below the level of x-ray diffraction detectability, however, nothing above background was indicated. This data again verifies that no appreciable SiAlON phase was formed in the deposited coating.

Figure 10 illustrates the appearance of a partly crystalline and partly amorphous 4-B coating after polishing. The 4-B coating group showed less tendency to crack and they were in general translucent to opaque. The color varied from light tan to dark brown and nearly black.

The grain structure of the group 4-B coatings was studied on fractured surfaces with the SEM. Some results are shown in Figure 11. While larger grains apparently coexist with smaller ones, grains as small as 1μ and less are distinguishable in Figure 11-b.

Figure 9. Scanning Electron Photomicrograph of Candidate Materials Set 4-B Coating known to Contain both Crystalline and Amorphous Characteristics

PP-40, Part 384-A at 330X

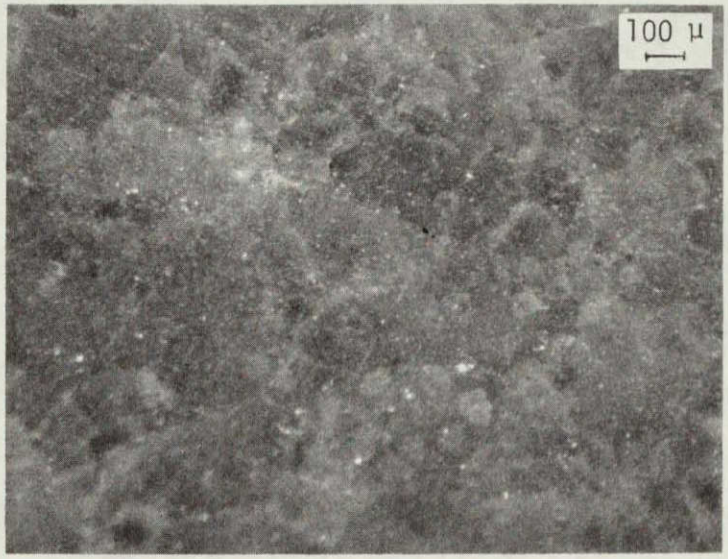

Figure 10. Optical Photomicrograph of Candidate Materials Set 4-B Coating Known to Contain Both Crystalline and Amorphous Characteristics

PP-40, Part 383-B at 52.5X, after polishing

a) 500X

b) 2500X

Figure 11. SEM photomicrographs of Candidate Materials Set 4-B Coating, Fractured Surface

Part No. 374-A, both photomicrographs from same region of sample, near polished face, all coating

2.4 CHARACTERIZATION AFTER SESSILE DROP EXPERIMENTS

The third quarterly report contained photomicrographs of fractured surfaces of molten silicon on CNTD SiC and Si_3N_4 and suggested that interfacial reaction was negligible. During the fourth quarter polished specimens were prepared and evaluated with optical microscopy, of CNTD SiC, Si_3N_4, and AlN interfaces with molten silicon.

2.4.1

First Candidate Materials Set - SiC

Figure 12 illustrates the stability of the interface between the silicon sessile drop and the CNTD SiC interface for Part No. 19, pp-26. The molten silicon had been in contact with the coated substrate at 1450°C for one hour. The dark spots in the silicon are believed to be polishing pull outs and not segregated grains of SiC.

Slight etching (Figure 12-b) sharpens the interface and confirms that the interdiffusion or reaction zone which must exist upon an atomic level is not of sufficient thickness to be identified at this intermediatly high magnification. Increased etching (Figure 12-c) provides no additional information concerning the interface but does, however, reveal some texture in the CNTD coating. The data presented in Section 2.1 of this report substantiates the authors analysis that the island like regions in the CNTD coating of Figure 12-c represent the action of the etchant rather than the ultimate grain size of the material.

The etchant was an aqueous solution of 5 wt% CrO_3 plus 1 wt% HF used electrolytically with a 10 volt positive potential on the specimen (anode).

The polished section evaluation supports fractures surface SEM results reported last quarter and the CNTD SiC material appears quite

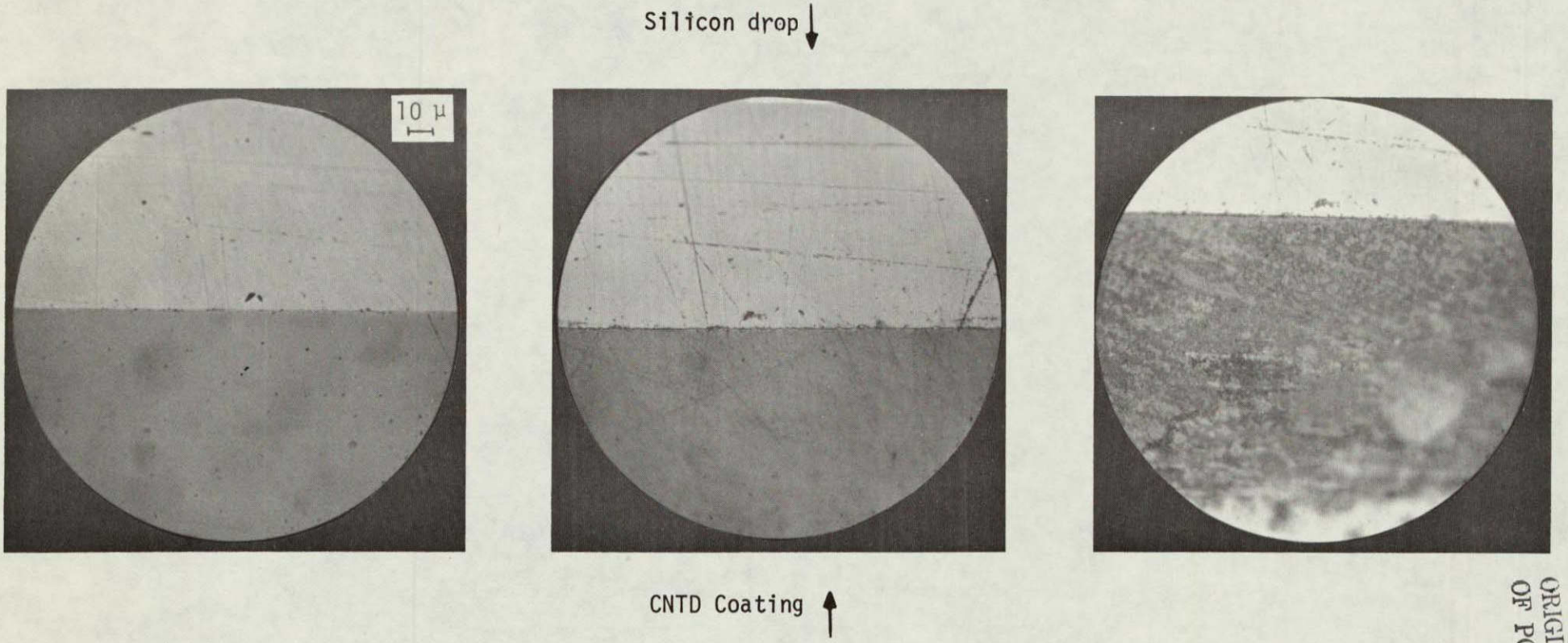

a) As Polished b) 10 Sec. Etch c) 30 Sec. Etch

Figure 12. Polished and Etched Cross Section of Silicon Sessile Drop for Interface Investigation

PP-26, Part No. 19, sessile drop run 1 hour at 1450°C, $10^{-18} > P_{O_2} > 10^{-24}$ electrochemical etch in aqueous solution of 5 wt% CrO_3 plus 1 wt% HF, at 10 volts positive potential (anode) on the specimen, 400X

promising in terms of reaction resistance, coherence, and adherence to the hot pressed substrate.

2.4.2 Second Candidate Materials Set - Si_3N_4

The CNTD Si_3N_4 coating was applied to two types of substrates "pure" (99.9%) and "impure" (95-98%) Si_3N_4 substrates hot pressed with 4 wt% MgO as an additive. No appreciable differences were observed, in characterization of the as-deposited coating, which could be attributable to the hot pressed substrate (see third quarterly report).

The silicon drop has been observed to "pop loose" from the coated specimen during cool-down in some cases (see Figure 13) and at least partially separate in others (see Figure 14-a). The CNTD coating has been observed to partially separate from the hot pressed substrate in certain runs with the PP-30, "impure", substrate as shown in Figure 13-b. Sessile drop experiments have not proceeded far enough to establish the frequency of this phenomenon. The CNTD structure is shown to be coherent at this magnification.

Figure 14-a shows the partial separation of a silicon drop from a CNTD Si_3N_4 coating on a PP-33, "pure", substrate. The bonded section is shown at higher magnification in Figure 14-b. There appears to be a reaction layer on the order of 1.0 to 1.2 microns in thickness, in close agreement with UMR results (Section 3.4). It is noteworthy that no significant transport of Si_3N_4 particles into the silicon has been observed.

The effects of a crack in the CNTD Si_3N_4 structure are shown in Figure 15. The crack is assumed to be of a pre-existing type as no evidence of massive reaction is noted. The molten silicon was apparently drawn into the crack by capillary action.

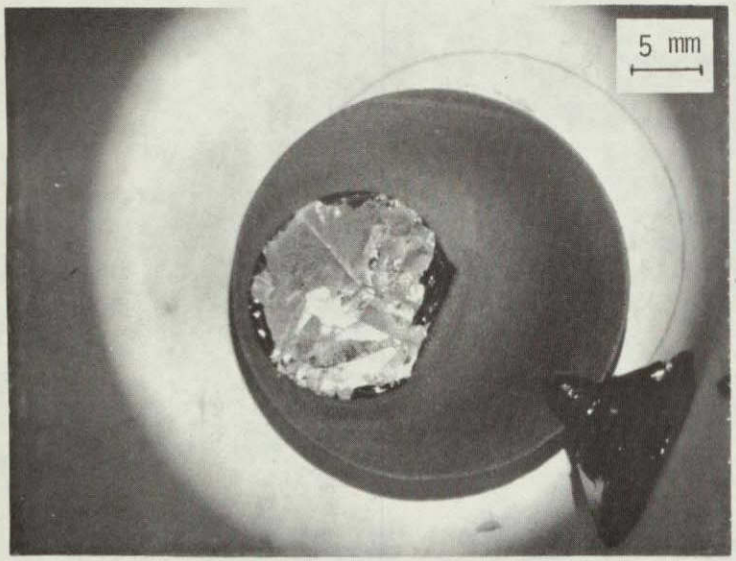

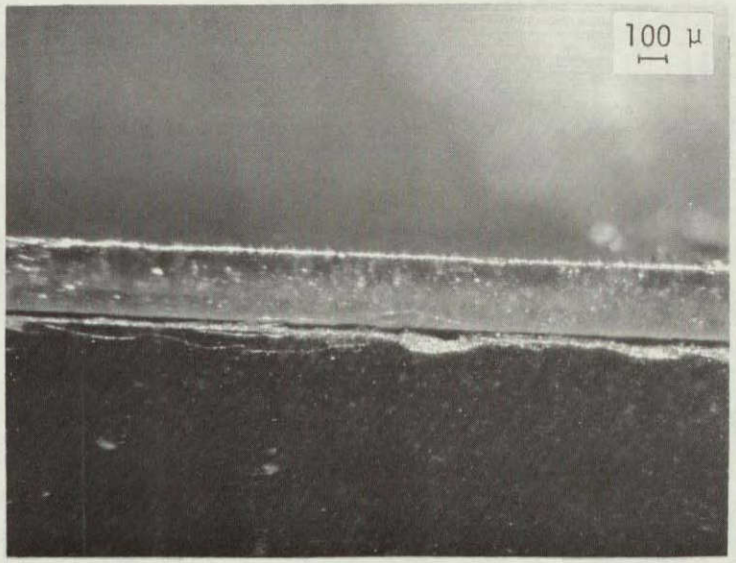

a) - 1.87X

b) - 34.5X

Figure 13. Post sessile Drop Conditions for CNTD Si_3N_4 on "Impure", PP-30, Si_3N_4 Substrate

PP-30, Part No. 3

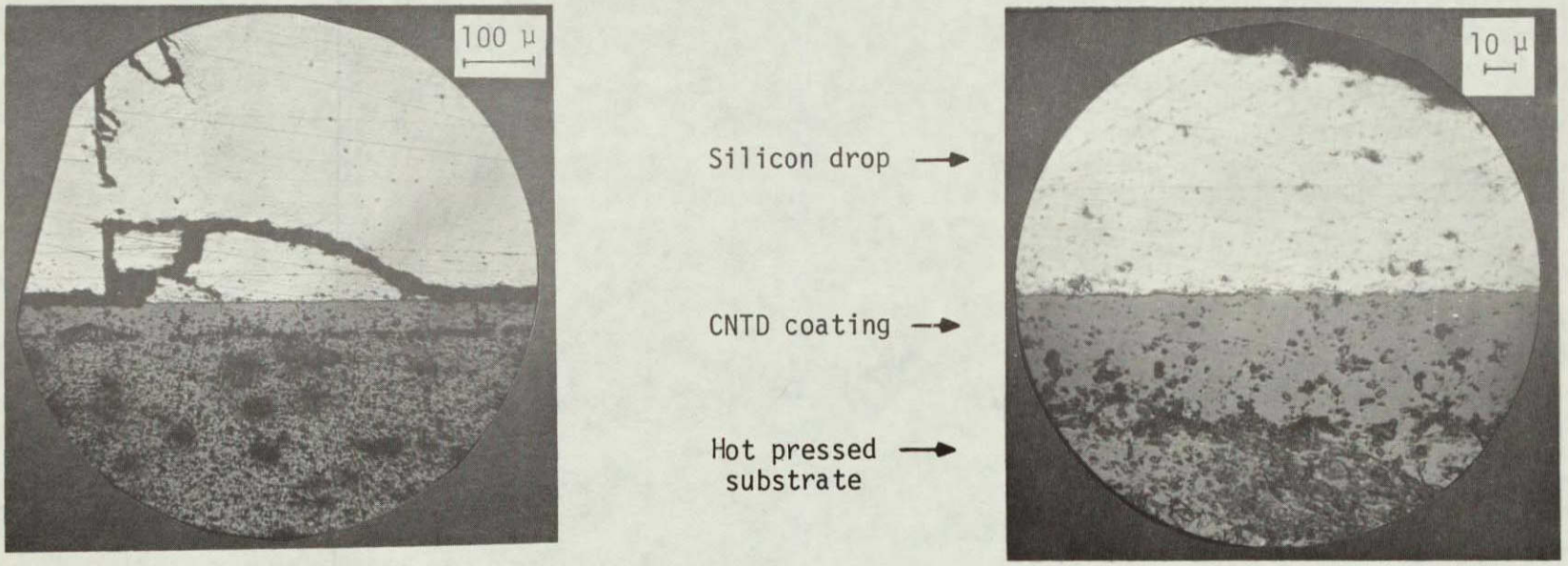

a - 100X

b-400X

Figure 14. Post Sessile Drop Conditions for CNTD Si_3N_4 on "Pure", PP-33, Si_3N_4 Substrate

PP-33, Part No. 5, 1 hour at 1450°C, $10^{-17} > P_{O_2} > 10^{-24}$

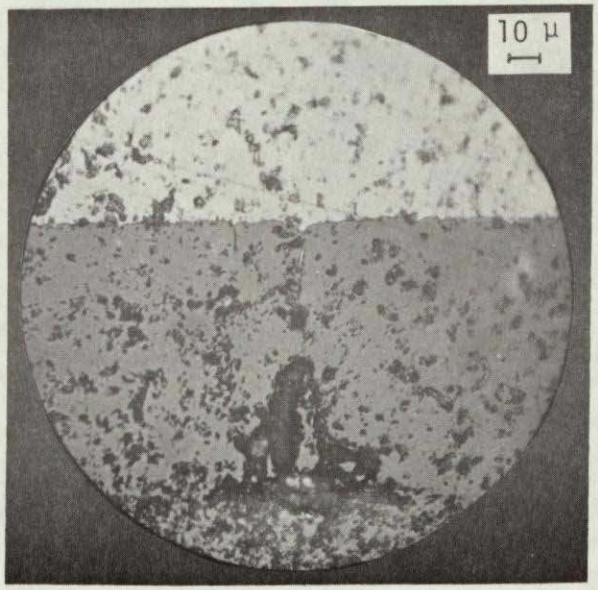

400X

Figure 15. The Effects of a Crack in the CNTD Coating

PP-33, Part No. 13, at 400X, 1 hour at 1450°C, $P_{O_2} \sim 10^{-17}$

The apparent voids are believed to be due to inadequate polishing.

These results are in general encouraging with respect to the ability of CNTD Si_3N_4 to resist molten silicon. Further evaluation of the effects of time at temperature, oxygen partial pressure, and CNTD coating/substrate considerations will be required for a full understanding of this material's viability.

2.4.3 Third Candidate Materials System - AlN

The system of CNTD AlN on hot pressed AlN has been given only a cursory evaluation in the sessile drop apparatus to date. The results are shown in Figure 16. The 400X photomicrograph shows that the molten silicon has penetrated the rather thin CNTD coating (approximately 25μ) and AlN material has been separated from the coating and migrated into the silicon.

While the results are not encouraging under these run conditions ($P_{O_2} \sim 10^{-17}$) the study of the effects of oxygen partial pressure may lead to an optimization of this material's usefulness.

2.5 DIE AND CRUCIBLE FABRICATION

The crucible hot pressing development began with prototypes 1 1/2" O.D. x 3/4" I.D. x 1 1/4" deep x 1 5/8" overall height, and densities of 90 to 95 percent of theoretical were obtained (see third quarterly report). The next stage of development was to press a larger and thinner walled crucible for contractual delivery requirements. The full size crucibles of the second candidate materials system, Si_3N_4, were hot pressed in September. (This was the system

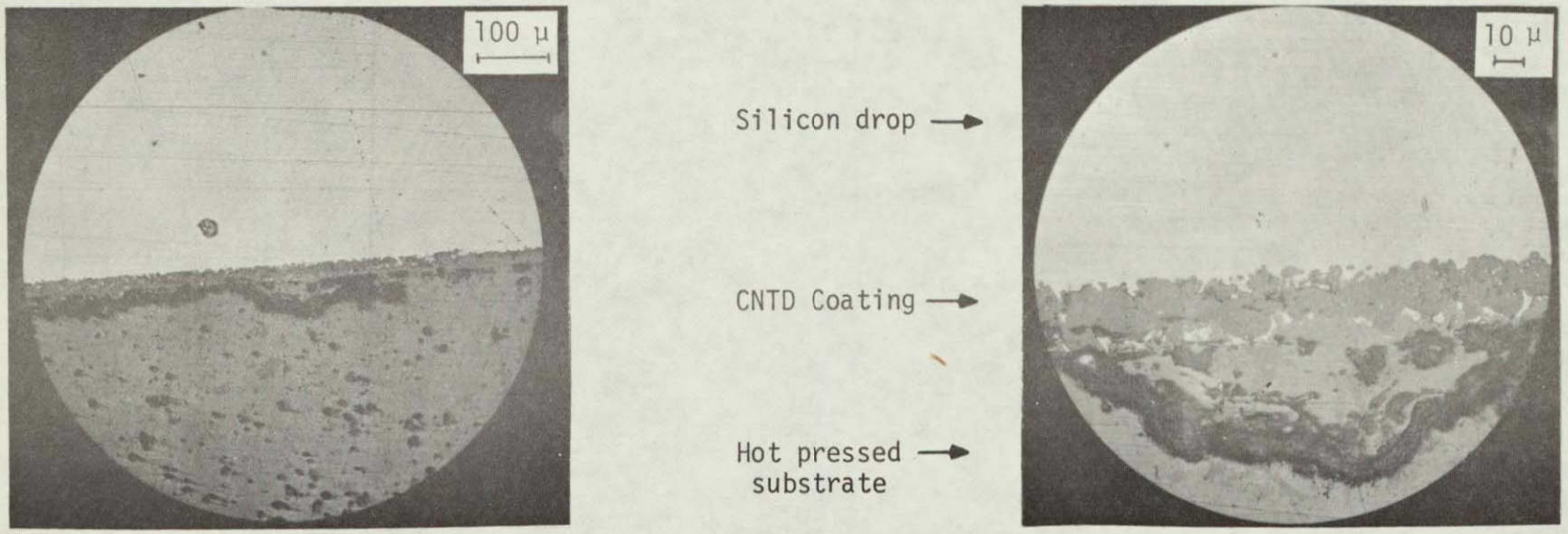

a) - 100X

b) - 400X

Figure 16. Polished Section of Interface Between Silicon Sessile Drop and CNTD AlN on Hot Pressed AlN Substrate.

AlN Part No. 1, 1 hour at 1450°C, $P_{O_2} \sim 10^{-17}$

hot pressing temperature was 1775 to 1785^{o}C and the applied pressure was 2400 lb/in^{2} (calculated from the pressing load in pounds divided by the total area defined by the crucible O.D.) Total run time was from 65 to 95 minutes with 15 to 20 minutes of that time utilized in increasing temperature and pressure. The final densities ranged from 90.3 to 92.8% of theoretical.

One full scale crucible was pressed from SiC with 1 wt% B, PP-26, and the results were encouraging. Development will continue in the fifth quarter.

The hot pressing of die blanks was straightforward. These were produced from "pure" Si_3N_4 with 4 wt% MgO, PP-33, at 1785 to 1790^{o}C, 4375 lb/in^{2}, and total run times of approximately 35 minutes. Approximately 15 minutes of that time was utilized in increasing temperature and pressure. Final densities ranged from 94.7 to 97.0 percent of theoretical. Grinding operations will be discussed in the next quarterly report.

3. UMR EFFORTS

Meaningful sessile drop measurements to elucidate the effects of oxygen partial pressure on the interaction between molten silicon and CNTD coated Si_3N_4, SiC and AlN substrates require that two measurements, namely, oxygen partial pressure over the sessile drop and the temperature of the drop-coating-substrate set be very precise. The results of this quarterly research period of UMR thus include:

1) Reconstruction and calibration of a ThO_2 - 7 wt% Y_2O_3 solid electrolyte cell which attains the capability to measure the P_{O_2} in the range from 10^{-6} to 10^{-30} atm.

2) Calibration of the optical pyrometer including the absorption correction due to the pyrex view-port in the sessile drop furnace.

3) Continuation of the sessile drop experiments.

4) Characterization of the molten Si/CNTD layer interaction employing Auger electron spectroscopy and optical and scanning electron microscopy and the establishment of standard characterization procedures to yield the desired information.

3.1 MEASUREMENT OF OXYGEN PARTIAL PRESSURE

The techniques for determining the oxygen content in liquid metal/metal oxide systems by galvanic cell has long been known (4-9). Ultra low P_{O_2} measurement in a flowing gas buffered system, however, is complicated since small variations of the gas flow rate in some ranges affect the heat exchange, the degree of reaction, and the temperature making it extremely difficult to determine the exact P_{O_2} from the galvanic output of the cell under such circumstances. The initial step

in the oxygen partial pressure measurement was to construct an oxide cell possessing a P_{O_2} sensitivity in the range of 10^{-6} to 10^{-30} atm. A second step effort was aimed at overcoming the inherent difficulties in measuring such low P_{O_2} values in a buffered flowing gas system. A third step involves calibrating and developing the full potential of this P_{O_2} measurement system.

3.1.1 ThO_2 - 7 wt% Y_2O_3 Solid Electrolyte Cell

The key factors in adopting a solid solution of ThO_2 - 7 wt% Y_2O_3 as the electrolyte were the high temperature stability of this material and its wide range of P_{O_2} measurability, i.e. the wide range over which an ion transference number of unity is obtained as shown in Figure 17. The P_{O_2} measuring system built in the UMR laboratory (Figure 18) consists of a horizontally oriented, dense Alumina (Al_2O_3) tube 1 3/4" O.D. x 1 1/2" I.D. x 25" long,(A) enclosing a ThO_2 - 7 wt% Y_2O_3 tube, closed at one end, 3/8" O.D. x 9/32" I.D. x 12" long.(B) Special shaped flanges and o-rings, (C) were employed to seal the tubes in the system and providing the gas inlet and outlet connections, (D to G) a thermocouple, (H) was installed from the experimental gas outlet (E) so that it would touch the tip of the ThO_2 - 7 wt% Y_2O_3 tube and measure the temperature at the exact point on the tube where the galvanic EMF was produced. The reference gas and the calibration CO/CO_2 gas or unknown gas (experimental gas) to be measured pass separately on opposite sides of the solid electrolyte wall. The furnace is operated in the 950-1100°C temperature range during the P_{O_2} measuring procedure. The galvanic EMF output from the cell and the thermoelectric output from

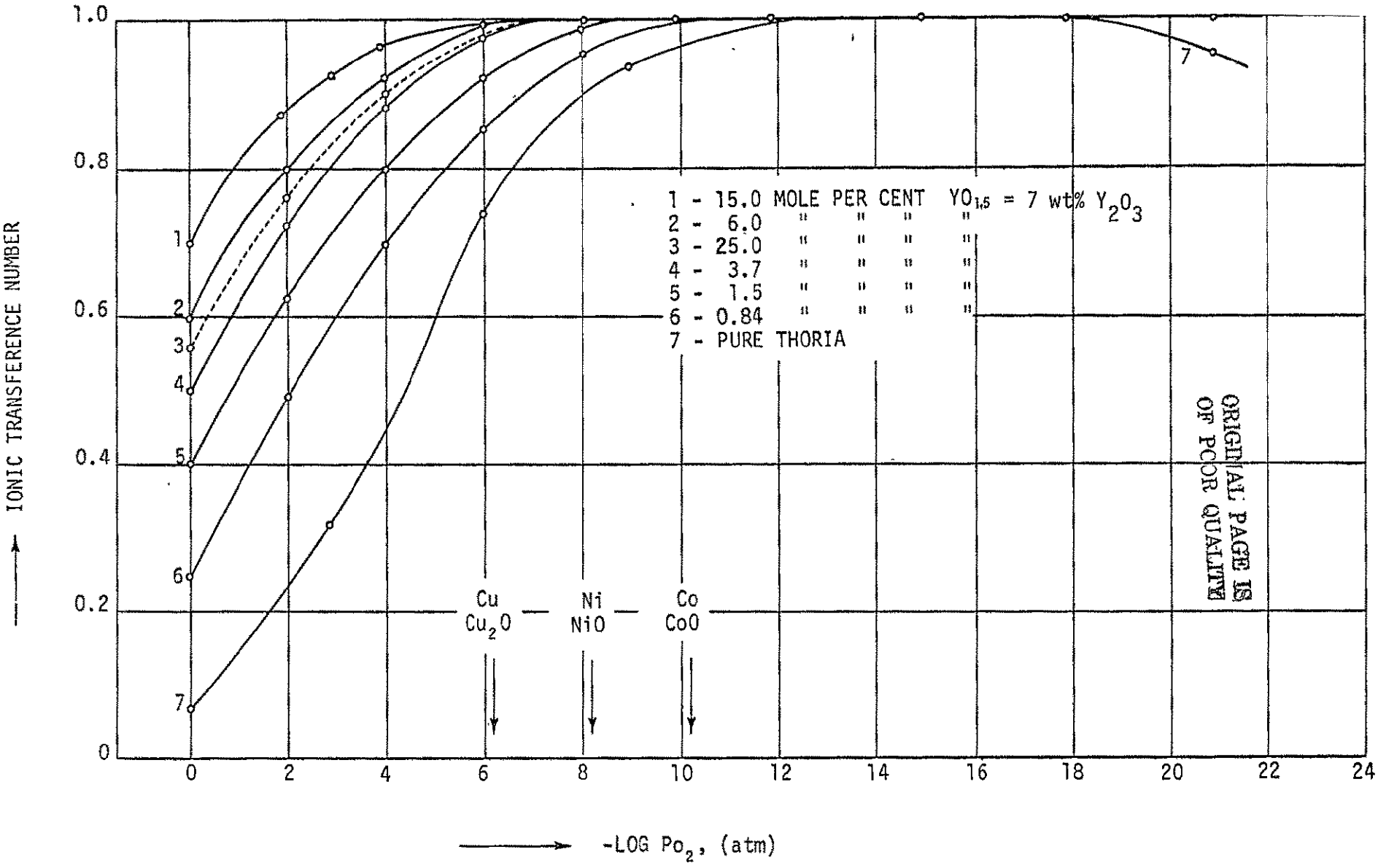

Figure 17. Ionic Transference Numbers in Pure Thoria and Thoria Base Solid Solution with Yttria as a Function of Oxygen Partial Pressure at 1000°C (reference 10)

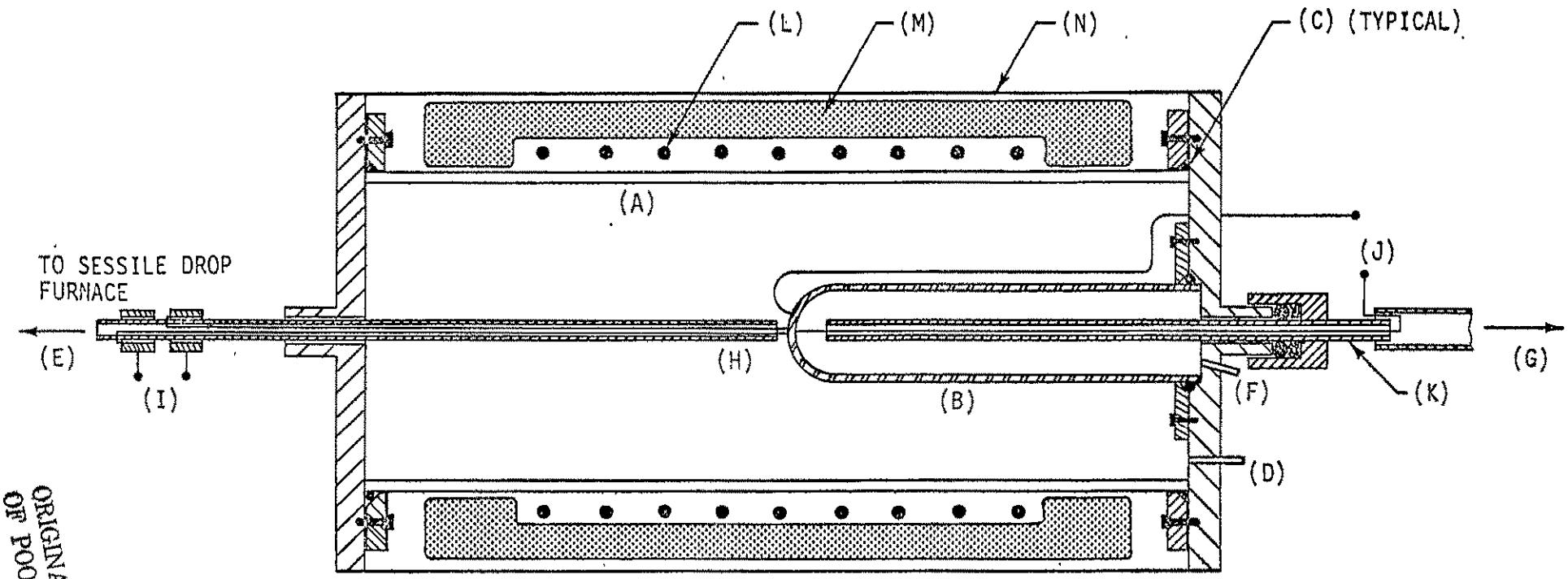

Figure 18. Apparatus for P_{O_2} Measurement

(A) Al_2O_3 tube, (B) ThO_2-7wt%Y_2O_3 tube, (C) Flange and o-ring seals, (D) Experimental gas inlet, (E) Experimental gas outlet, (F) Reference gas inlet, (G) Reference gas outlet, (H) Thermocouple, (I) Thermocouple output, (J) Cell galvanic EMF output, (K) Al_2O_3 gas carrier tube with galvanic lead, (L) Heating element, (M) Insulation, (N) Metal shell

the thermocouple are measured at points (J) and (L) respectively with differential digital potentiometers.

3.1.2 Method to Overcome the Flow Rate Effects

The relationship between the reference gas flow rate and the galvanic output at a fixed flow rate (600 cc/min) of CO/CO_2 has been explored and is presented in Figure 19. It is found that the EMF is essentially independent of reference gas flow rate for values of the flow meter reading greater than 130. The EMF output is also found to be insensitive to the rate of gas flow outside the tube in the range of interest (600 cc/min) provided the reference gas flow rate is set within the EMF independent range at a meter reading of 140. The adverse effects of gas flow rate were aleviated by calibrating the galvanic output with respect to these optimum flow rates for reference gas and calibration gas. The P_{O_2} in an unknown gas at this flow rate could therefore be evaluated using this calibration curve.

3.1.3 A Known P_{O_2} Atmosphere Source - CO/CO_2 Buffering System

From the previous section, it is clear that a known P_{O_2} atmosphere is essential for the calibration of a gaseous P_{O_2} measuring system. A CO/CO_2 buffering system controlled by a proportional flow meter was employed to meet this requirement. By fixing the CO/CO_2 ratio and temperature a known P_{O_2} atmosphere is established. This can also be seen from the mass action law, $P_{CO_2} \cdot P_{CO}^{-1} \cdot P_{O_2}^{-\frac{1}{2}} = K$, for the reaction $CO + 1/2\ O_2 \rightleftarrows CO_2$. The range of P_{O_2} offered by the

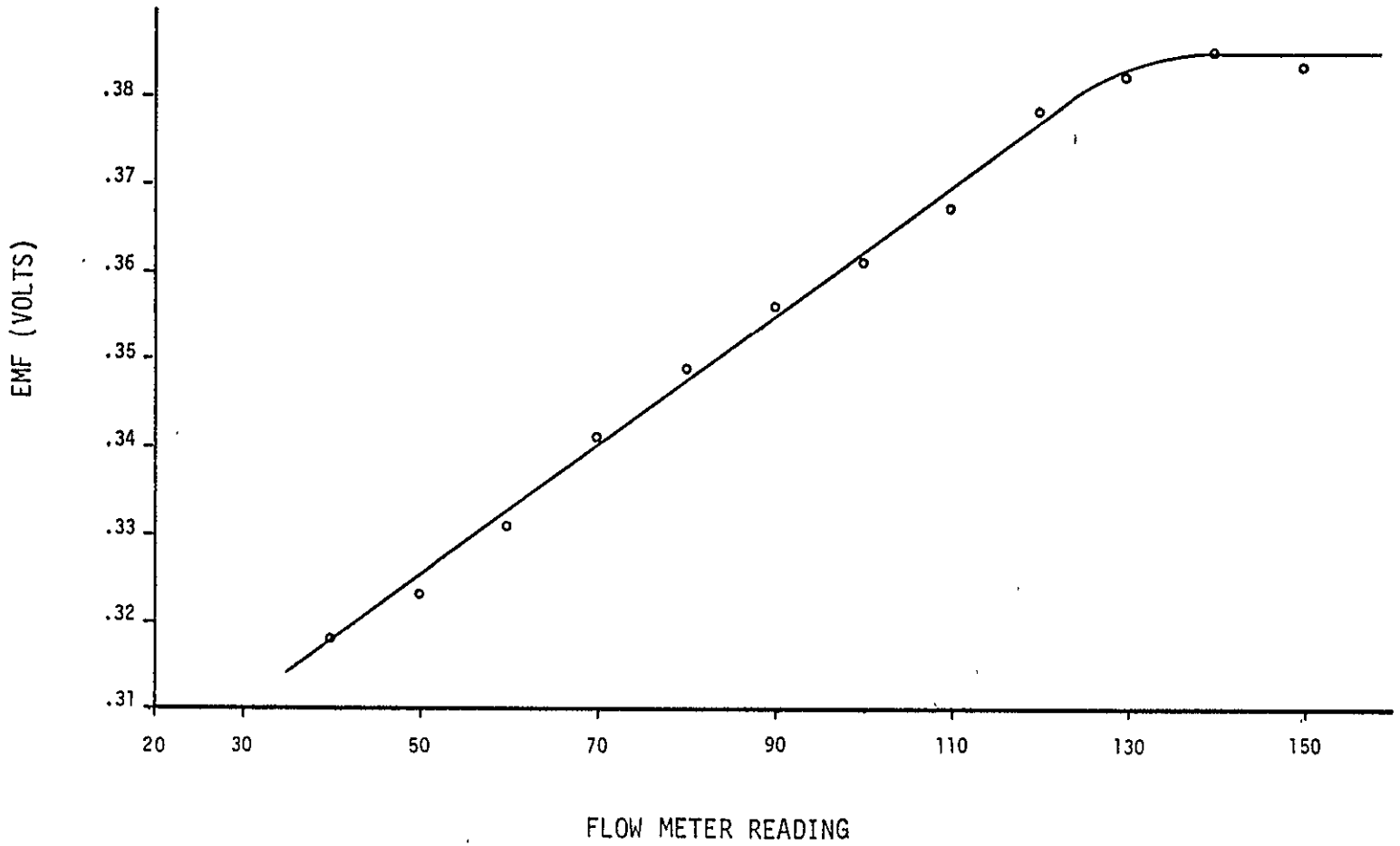

Figure 19. Effect of Reference Gas Flow Rate on Galvanic EMF Output from the Cell at a Fixed CO/CO_2 gas Flow Rate. (600 cc/min).

CO/CO_2 buffering system, however, is limited. Carbon will "soot out" as the P_{O_2} is reduced to the point where it will be dominated by the $C + 1/2\ O_2 \rightleftarrows CO$ equilibrium.

3.1.4 Calibration and Development of the Oxide Cell

By varying the CO/CO_2 ratio to yield different P_{O_2} atmospheres, calibration data of the oxide cell at fixed gas flow rates were obtained at 1000°C and 1100°C and are presented in Table V. The least squares slopes in the linear plots of log P_{O_2} vs EMF (Figure 20) are calculated to be 0.030 and 0.029 at 1000°C and 1100°C respectively, which are very close to the theoretical values of 0.027 and 0.030.

The close agreement between the theoretical and experimental data establishes the validity of the data from this oxide cell and justifies the extrapolation necessary to determine the P_{O_2} of a gas below the limit of the CO/CO_2 buffer.

3.2 TEMPERATURE CALIBRATION

Deviation of the experimental temperature readings from the published silicon melting point had been observed and has led to serious consideration of the accuracy of the optical pyrometer and the necessity of correcting the reading due to absorption by the pyrex view-port. A model #105 optical pyrometer calibrating set was employed to provide a reliable temperature source which could be adjusted to a desired temperature nearly instantaneously. The relation between the brightness (wave length 0.65 microns) of the filament at a certain temperature and the lamp current was furnished (Table VI) with the certificate of calibration from NBS. The readings of the pyrometers were first adjusted to the standard temperature by the following

TABLE V

Galvanic EMF Output From the ThO_2 - 7 wt% Y_2O_3 Solid-Electrolyte Cell for Various Oxygen-Partial-Pressure Atmospheres

The flow rate of reference gas is kept at 140 of the flow meter reading. In the expression, R is the CO/CO_2 ratio.

	log R	-log P_{O_2}	EMF (Volts)
1000°C	1.8	17.5	0.22
	1.3	16.6	0.253
	0.8	15.7	0.296
	0.3	14.7	0.361
	0.17	14.4	0.382
	-0.2	13.7	0.473
	-0.2	13.6	0.47
	-1.15	12.7	0.54
1100°C	1.8	16.1	0.23
	1.3	15.1	0.28
	0.8	14.1	0.33
	0.3	13.1	0.401
	0.17	12.9	0.425
	0.08	12.7	0.45
	0.0	12.5	0.49
	-0.3	12.0	0.526
	-0.47	11.1	0.58
	-0.74	9.6	0.63
	CO_2 only	4.34	1.07

° – 1000° C

• – 1100° C

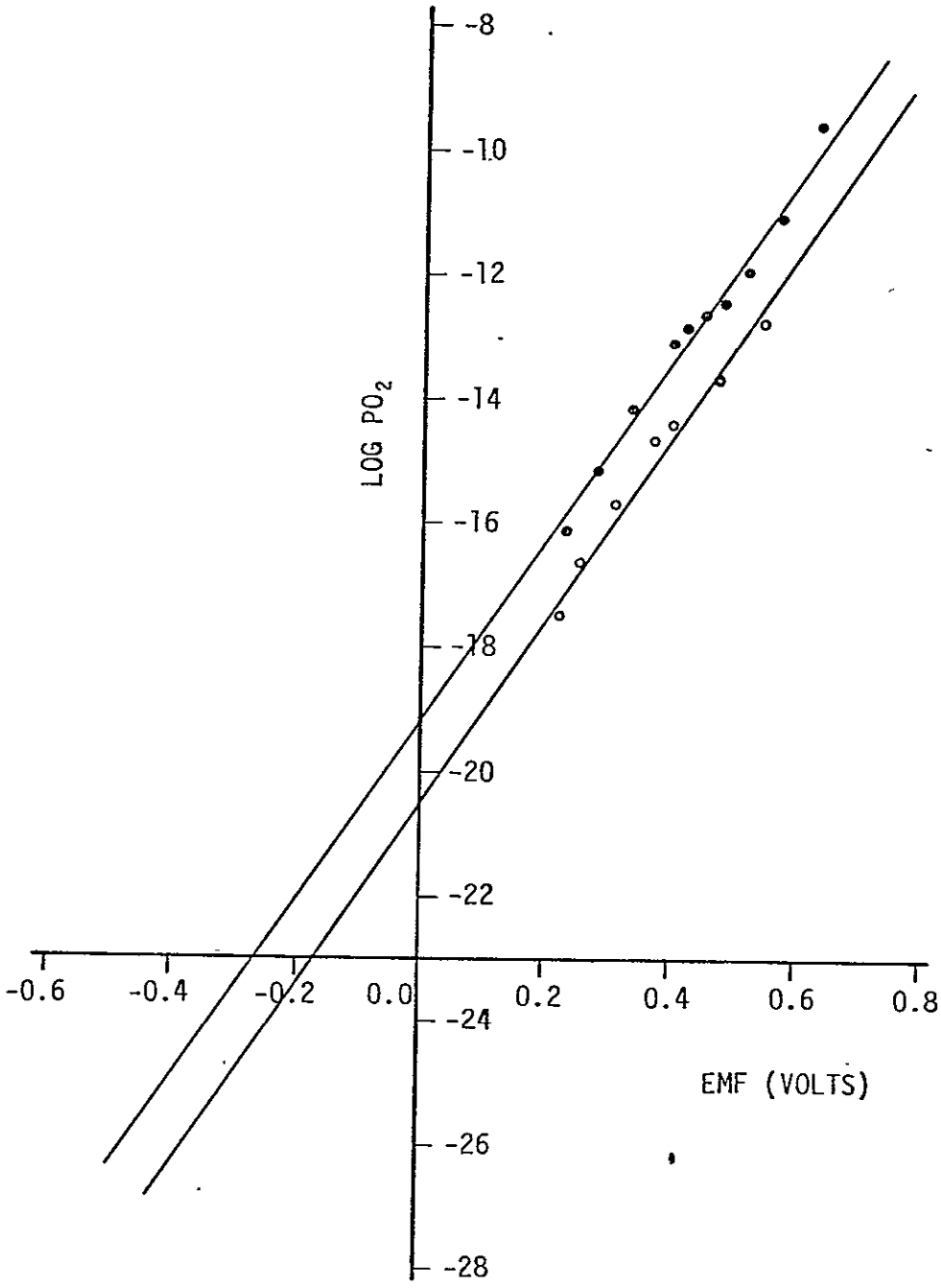

Figure 20. Relationship Between Log P_{O_2} and Galvanic EMF Output at 1000°C and 1100°C.

TABLE VI

Brightness Temperature[1] (at wave length 0.65 microns) as a Function of Lamp Current for Model No. 107 Calibration Set.

T (^{o}C)	Amperes	T (^{o}C)	Amperes
800	4.91	1600	10.21
900	5.315	1700	11.13
1000	5.795	1800	12.09
1100	6.38	1900	13.14
1200	7.02	2000	14.2
1300	7.725	2100	15.3
1400	8.51	2200	16.45
1500	9.34	2300	17.65

[1] At wavelength 0.65 μ

procedures: 1) the current in the ribbon filament lamp was set at a predetermined value, 2) the rheostat of the pyrometer was returned to the position at which the pyrometer filament matches the lamp filament in brightness, 3) the position of the rheostat was fixed, and 4) the reading of the pyrometer was adjusted to the corresponding temperature in Table VI.

Various filament temperatures were established in the lamp and the corresponding readings of the pyrometers are presented in Table VII. Correction temperatures (ΔT) for the absorption due to the pyrex viewport were calibrated at fixed filament temperatures by taking the difference in the temperature readings with and without the pyrex viewport. The resulting data are presented in Table VIII. The actual temperature of the sessile drop and substrate is obtained by adding the ΔT to the temperature reading through the viewport.

3.3 SESSILE DROP EXPERIMENTS

Because of the desire to establish the accuracy of the measurements of temperature and oxygen partial pressure, before using any more of the somewhat scarce coated specimens, the sessile drop test progress was limited to one experiment with CNTD Si_3N_4. The evaluation of this experiment and the sessile drop test specimens from late in the last reporting period, and also plans for tests to extract the most valuable information from the available specimens are in progress. The preliminary results submitted in the third quarterly report indicate that only a minimum reaction occurred in the molten silicon/CNTD SiC or Si_3N_4 interface after one hour as suggested by the clean interface revealed in the SEM pictures. The only observed silicon penetration was at the cracks in

TABLE VII. Calibration of Pyrometers' Reading to Reference Lamp Filament Temperature.

(A) Optical Pyrometer

Filament Temperature (^{o}C)	Pyrometer Reading (^{o}C)
1200	1200
1300	1298
1400	1399
1500	1490
1600	1600← High scale
1700	1699
1800	1800

(b) Micro Pyrometer

Filament Temperature (^{o}C)	Pyrometer Reading (^{o}C)
1200	1200
1300	1300
1400	14-0
1500	1500
1600	1594
1700	1700
1800	1795

TABLE VIII. Correction of the Pyrex Viewport Absorption at Various Temperatures.

Temperature (^{o}C)		
Without Viewport	With Viewport	ΔT
1200	1190	10
1298	1286	12
1399	1386	13
1490	1475	15
1600	1579	21
1700	1680	20
1800	1775	25

some Si_3N_4 coatings, (Figure 21). Longer time and higher temperature experiments will be made on both of these materials to determine the minimal reaction limits.

3.4 CHARACTERIZATION

In characterizing a post-sessile-drop test-sample to evaluate it's potential in serving as a die and/or container material for large area silicon sheet growth, the contamination of the silicon from the contact with the coated surface and the degradation of the ceramic coated substrate are the two most important aspects to be considered. As an initial screening step, SEM images of the fractured surface and optical micrographs of the polished surface are employed to define the degree of interface reaction and possible precipitation. Detection of the details of the degree of chemical reaction, however, is more complicated and presents some problems in Si_3N_4 and SiC. For chemical reaction in the micron range, profiling composition along the vertical cut edge would yield sufficient information. For the submicron chemical reaction Auger electron spectroscopy techniques utilizing depth profiling of the composition through the interface are necessary. This is being done primarily by sputtering surface atoms with an ion beam and analyzing the composition at the bottom of the ion crater at various sputter depths.

Silicon, aluminum, and nitrogen concentration changes are easily measured and distinguished in sessile drop experimental AlN coated samples. However, in the SiC and Si_3N_4, silicon is a major atomic species requiring more sophistication in reaction profiling, relying on more qualitative chemical shift information to define the chemical interaction and silicon penetration.

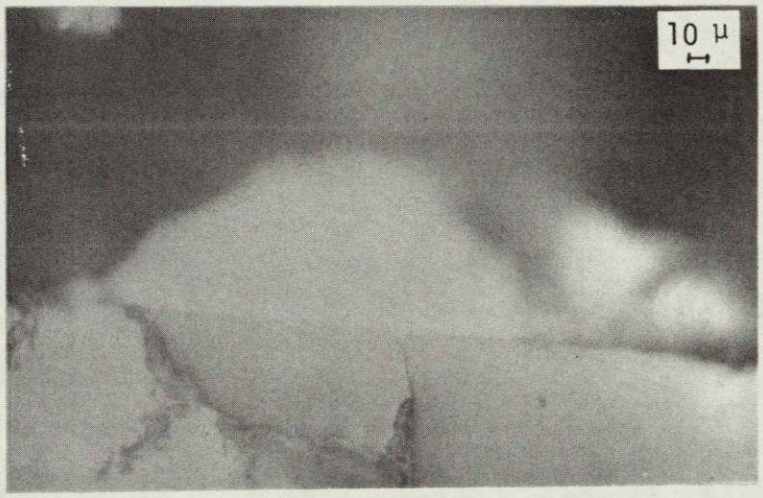

Figure 21. Silicon Penetration of a Crack in a CNTD Si_3N_4 Coating, 250X

A typical characterization of the interaction of molten silicon with a CNTD Si_3N_4 coating after one hour at 1430°C under very low oxygen partial pressure conditions are presented in Figure 22 in a series of incremental surface analyses. Even though the detailed molten silicon penetration information is not significant in this result, the relative depth of the chemical reaction zone between molten silicon and the CNTD Si_3N_4 coating is suggested from this analysis. The dN/dE peaks for carbon and nitrogen in the Auger spectrum are utilized to mark the reaction zones in Figure 23. The nearly constant heights in C and N peaks of Auger spectra detected in the region at and before 4 minutes sputtering and the region at and beyond 126 minute sputtering indicate that these regions are the molten silicon zone and the nonreacted substrate region, respectively. By taking the sputtering rate to be approximately as 45-60 Å/minute, the thickness of the chemical reaction zone, which lies between these two regions, is estimated to be in the range of 0.5 to 0.7 microns. This submicron chemical interaction between molten silicon and CNTD Si_3N_4 is consistent with the clear interface observed in SEM and optical photomicrographs. The CNTD Si_3N_4 coating thus appears to be a candidate for the container and die material in the LSSA task.

Preliminary Auger analysis of post silicon sessile drop test CNTD AlN coatings (Figure 24) indicates a high silicon resolution ability in AlN and that detailed information about the silicon penetration in this material is certainly attainable. An analysis of the silicon drop surface composition in the region near the drop/coating interface was

PHYSICAL ELECTRONICS INDUSTRIES
AUGER CHART 471083

Figure 22-a. Post Sessile Drop Auger Electron Surface Analysis CNTD Si_3N_4

Silicon rich region just above interface-before sputtering.

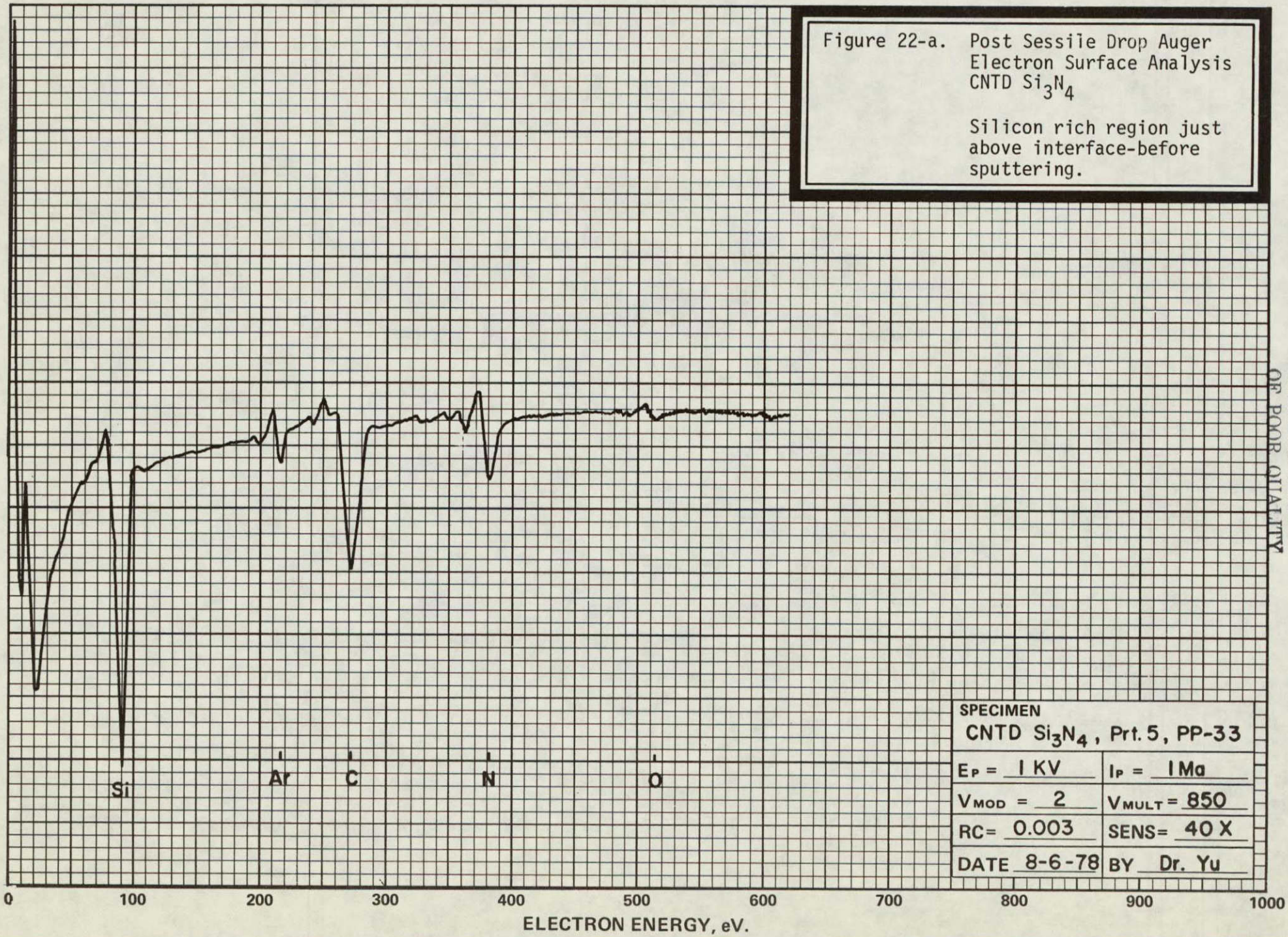

SPECIMEN CNTD Si_3N_4, Prt. 5, PP-33	
E_P = 1 KV	I_P = 1 Ma
V_{MOD} = 2	V_{MULT} = 850
RC= 0.003	SENS= 40 X
DATE 8-6-78	BY Dr. Yu

PHYSICAL ELECTRONICS INDUSTRIES
AUGER CHART 471083

Figure 22-b. Post Sessile Drop Auger Electron Surface Analysis CNTD Si_3N_4

After 4 min. sputtering

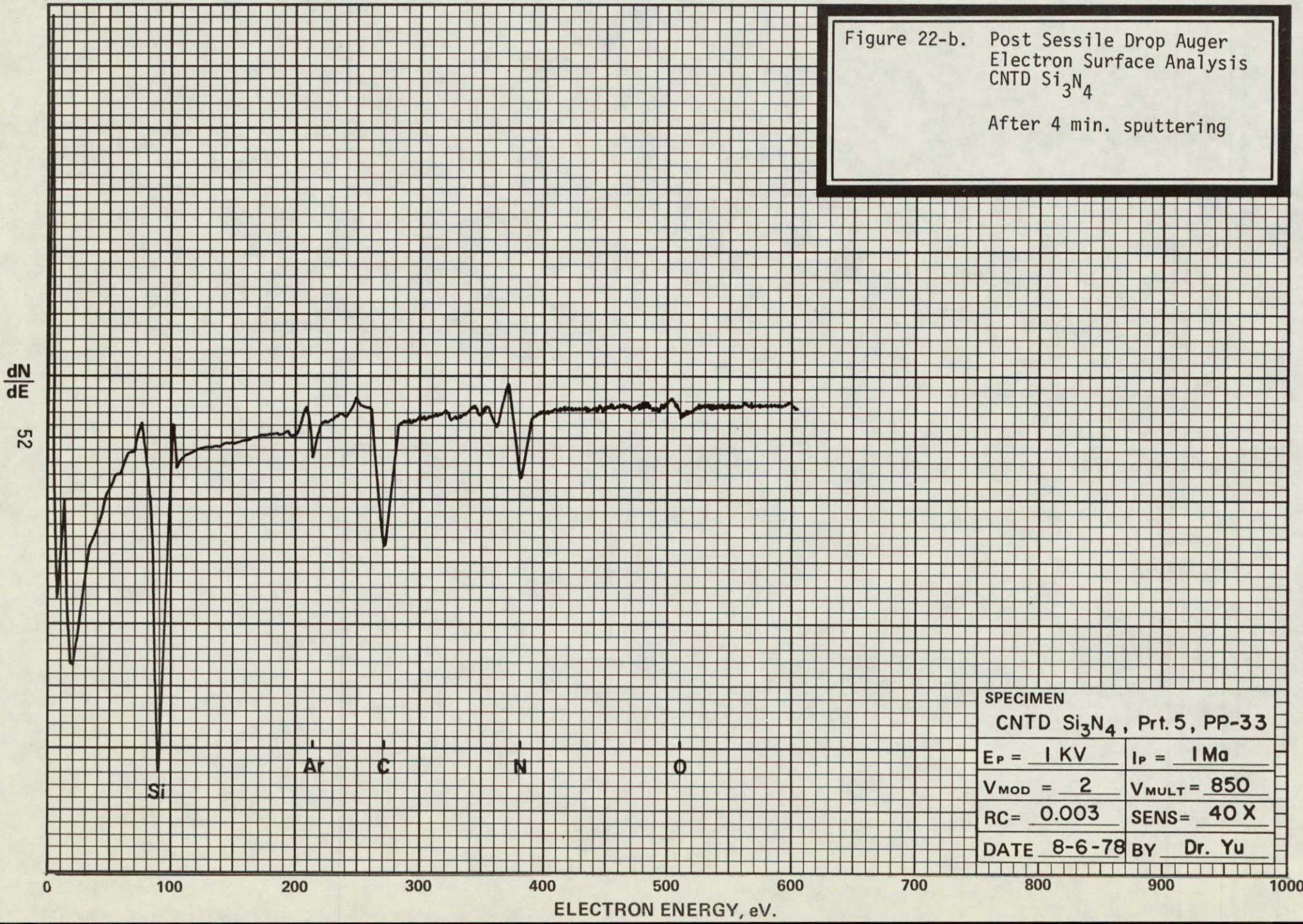

SPECIMEN	
CNTD Si_3N_4, Prt. 5, PP-33	
E_P = 1 KV	I_P = 1 Ma
V_{MOD} = 2	V_{MULT} = 850
RC= 0.003	SENS= 40 X
DATE 8-6-78	BY Dr. Yu

PHYSICAL ELECTRONICS INDUSTRIES
AUGER CHART 471083

Figure 22-c. Post Sessile Drop Auger Electron Surface Analysis CNTD Si_3N_4

After 10 min. sputtering

SPECIMEN CNTD Si_3N_4, Prt. 5, PP-33	
E_P = 1 KV	I_P = 1 Ma
V_{MOD} = 2	V_{MULT} = 850
RC= 0.003	SENS= 40 X
DATE 8-6-78	BY Dr. Yu

dN/dE

0 100 200 300 400 500 600 700 800 900 1000

ELECTRON ENERGY, eV.

PHYSICAL ELECTRONICS INDUSTRIES
AUGER CHART 471083

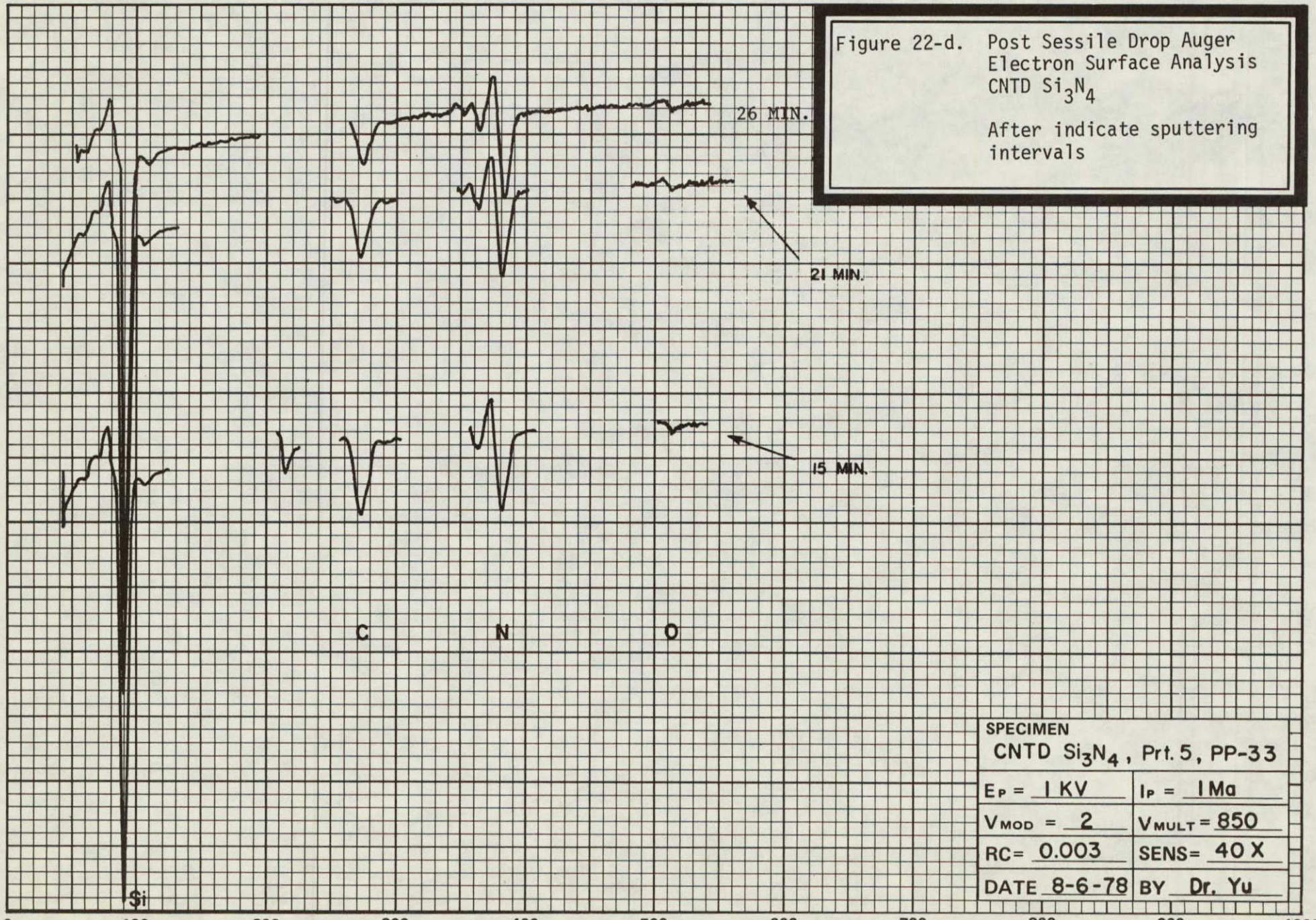

Figure 22-d. Post Sessile Drop Auger Electron Surface Analysis CNTD Si_3N_4

After indicate sputtering intervals

SPECIMEN CNTD Si_3N_4, Prt. 5, PP-33	
E_P = 1 KV	I_P = 1 Ma
V_{MOD} = 2	V_{MULT} = 850
RC= 0.003	SENS= 40 X
DATE 8-6-78	BY Dr. Yu

PHYSICAL ELECTRONICS INDUSTRIES
AUGER CHART 471083

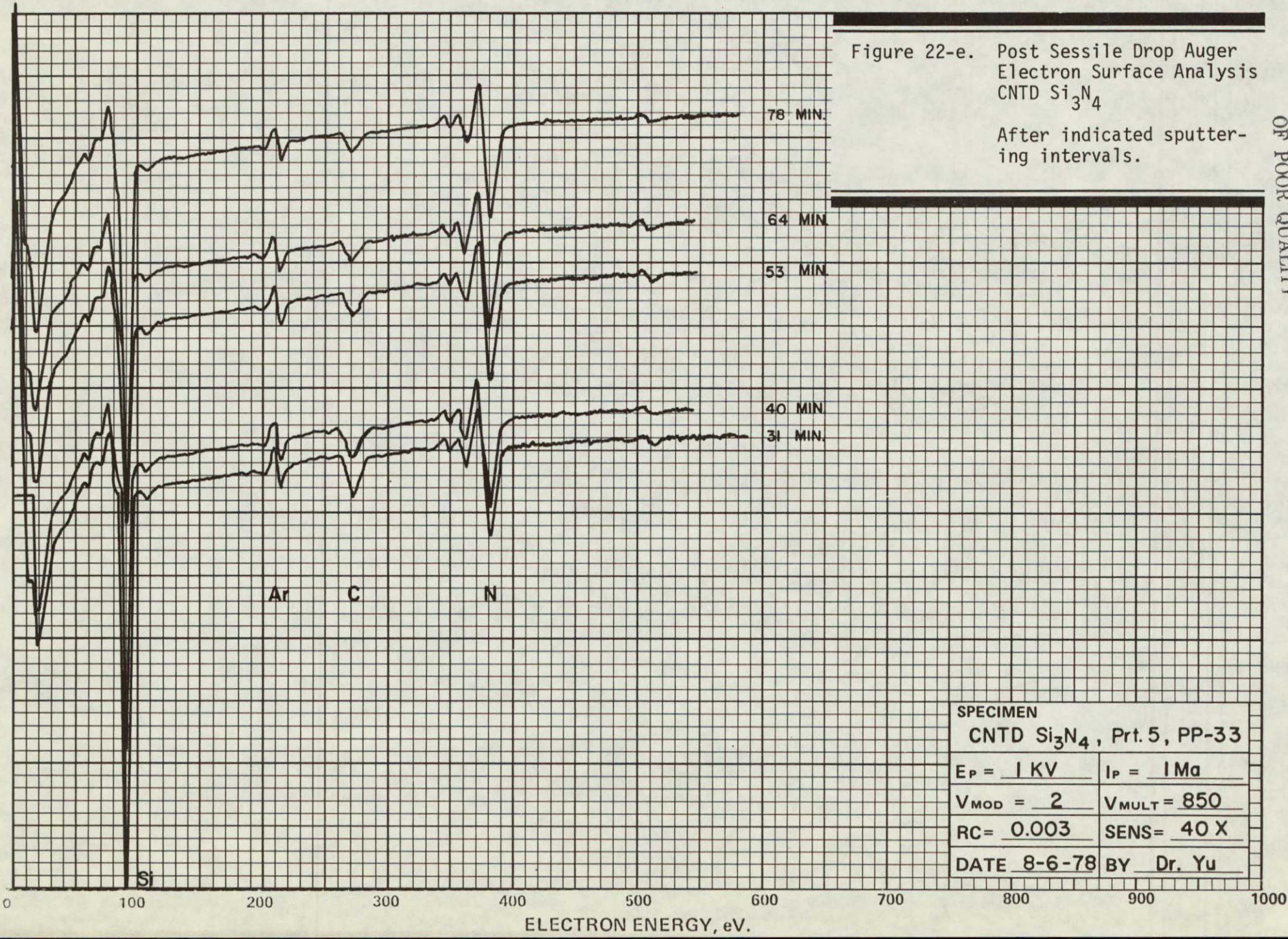

Figure 22-e. Post Sessile Drop Auger Electron Surface Analysis CNTD Si_3N_4

After indicated sputtering intervals.

SPECIMEN	
CNTD Si_3N_4, Prt. 5, PP-33	
E_P = 1 KV	I_P = 1 Ma
V_{MOD} = 2	V_{MULT} = 850
RC= 0.003	SENS= 40 X
DATE 8-6-78	BY Dr. Yu

PHYSICAL ELECTRONICS INDUSTRIES
AUGER CHART 471083

Figure 22-f. Post Sessile Drop Auger Electron Surface Analysis CNTD Si_3N_4

After 126 min. sputtering

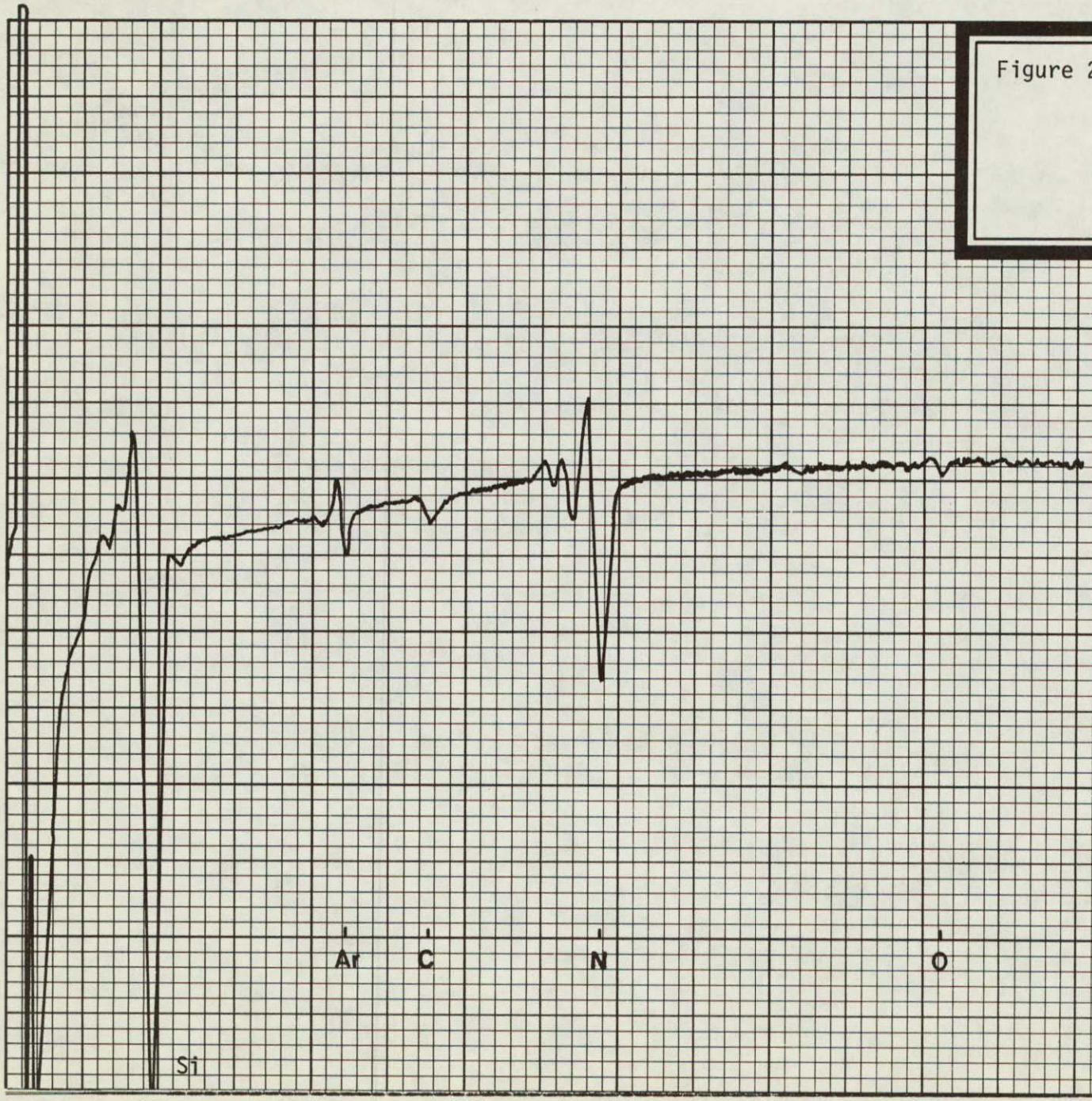

SPECIMEN	
CNTD Si_3N_4, Prt. 5, PP-33	
E_P = 1 KV	I_P = 1 Ma
V_{MOD} = 2	V_{MULT} = 850
RC= 0.003	SENS= 40 X
DATE 8-6-78	BY Dr. Yu

PHYSICAL ELECTRONICS INDUSTRIES
AUGER CHART 471022

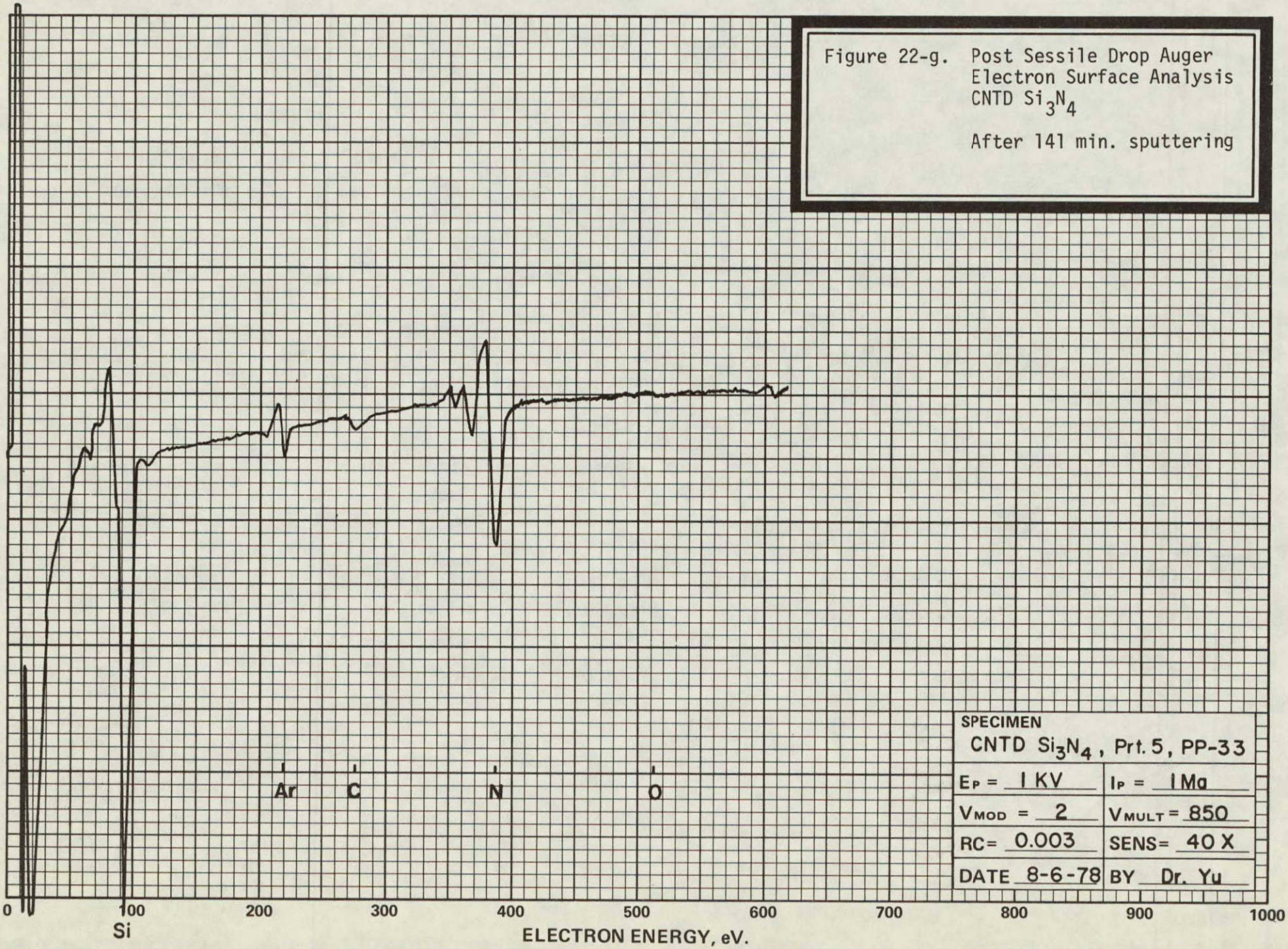

Figure 22-g. Post Sessile Drop Auger Electron Surface Analysis CNTD Si_3N_4

After 141 min. sputtering

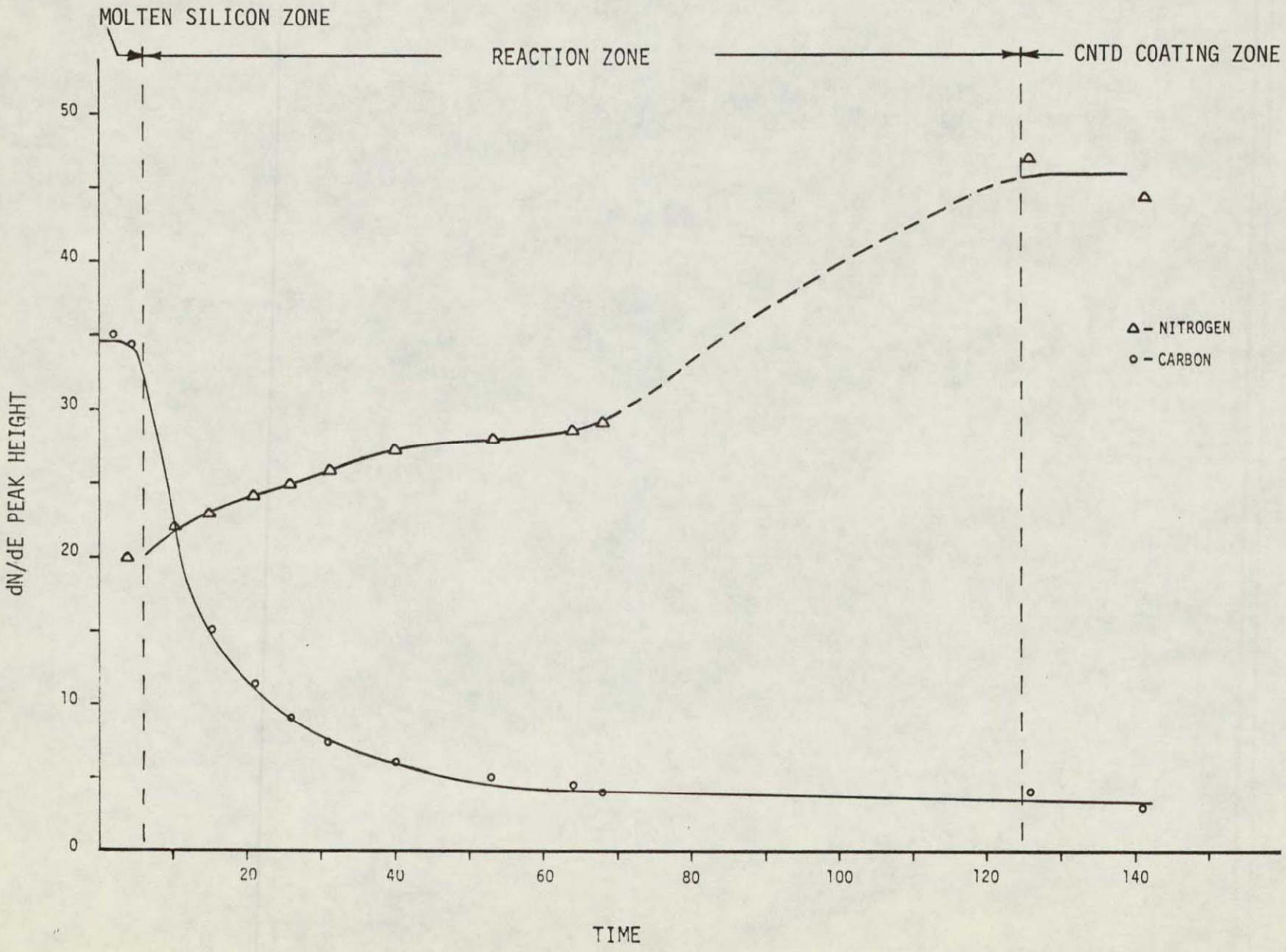

Figure 23. Variation of Carbon and Nitrogen dN/dE Auger Peaks With Time of Sputtering (ie. depth into interface) for Silicon on CNTD Si_3N_4.

PHYSICAL ELECTRONICS INDUSTRIES
AUGER CHART 471083

Figure 24-a. Post Sessile Drop Auger Electron Surface Analysis, CNTD AlN

After 2 min. sputtering

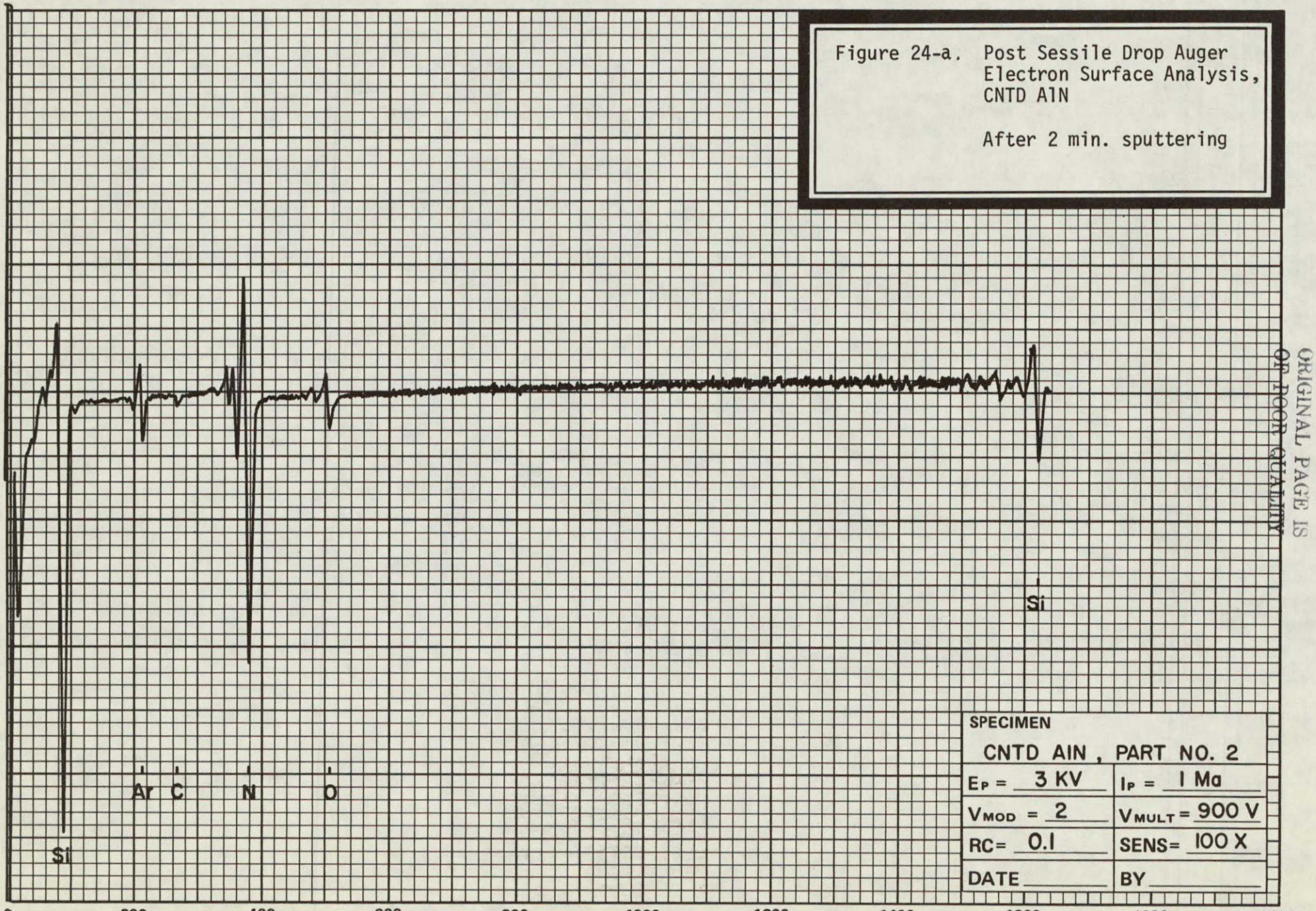

SPECIMEN	
CNTD AIN , PART NO. 2	
E_P = 3 KV	I_P = 1 Ma
V_{MOD} = 2	V_{MULT} = 900 V
RC= 0.1	SENS= 100 X
DATE	BY

PHYSICAL ELECTRONICS INDUSTRIES
AUGER CHART 471022

Figure 24-b. Post Sessile Drop Auger Electron Surface Analysis CNTD AlN

After 10 min. sputtering

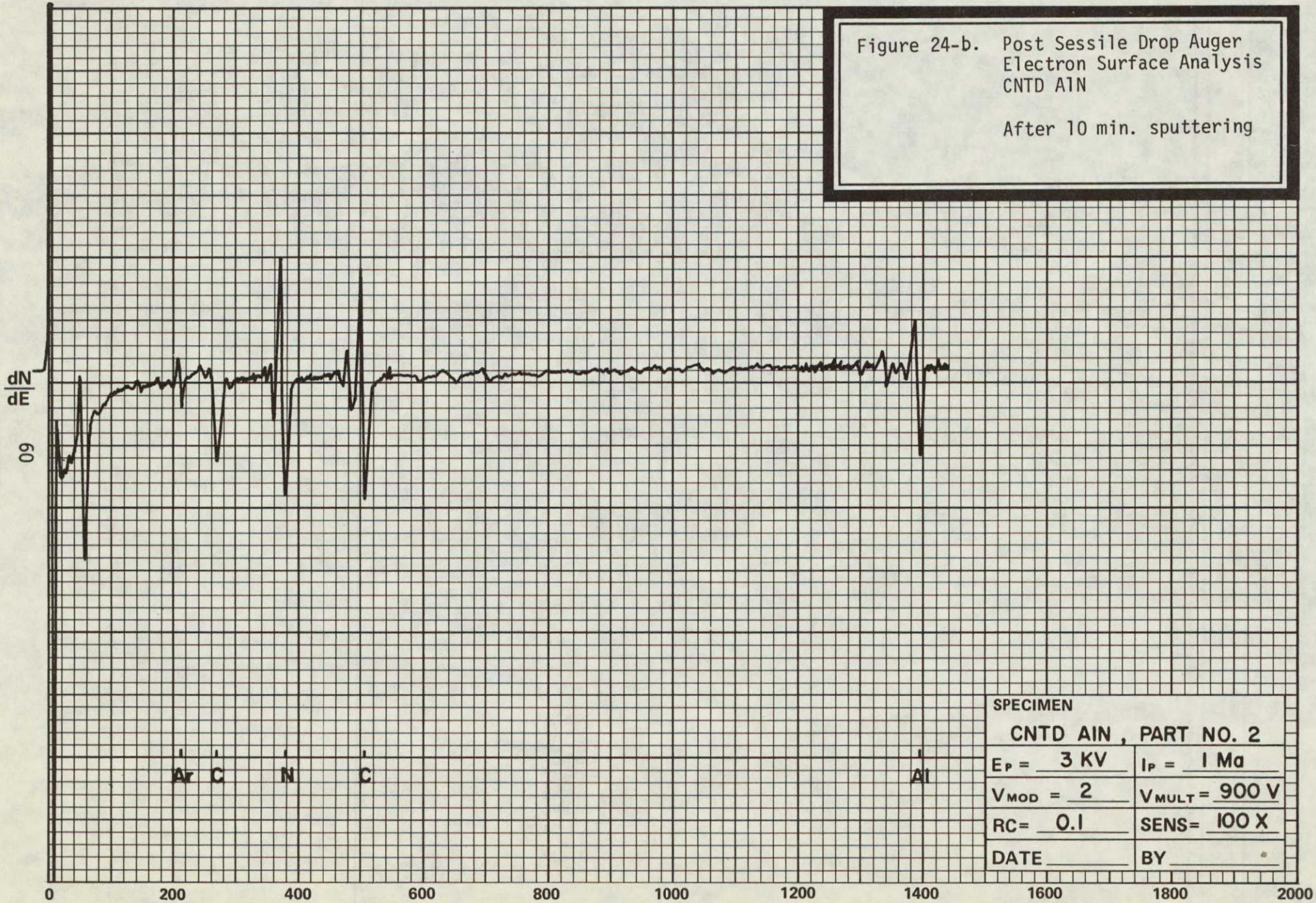

SPECIMEN	
CNTD AIN , PART NO. 2	
E_P = 3 KV	I_P = 1 Ma
V_{MOD} = 2	V_{MULT} = 900 V
RC= 0.1	SENS= 100 X
DATE	BY

obtained for each sputtering and are presented in Figure 25. A trend of increasing silicon and nitrogen peaks is observed. No sign of decreasing Si content and no Al signal were found after 87 minutes sputtering which implies that the probing is still within the molten silicon region. However, this deep penetration of nitrogen in molten silicon might indicate a significant chemical reaction between molten silicon and the CNTD AlN. More detailed experiments on this CNTD AlN are necessary to make a final comment on its compatability with the molten silicon.

PHYSICAL ELECTRONICS INDUSTRIES
AUGER CHART 471022

Figure 25-a. Auger Electron Analysis of Silicon Drop Melted on CNTD AlN

Near drop/coating interface - before sputtering

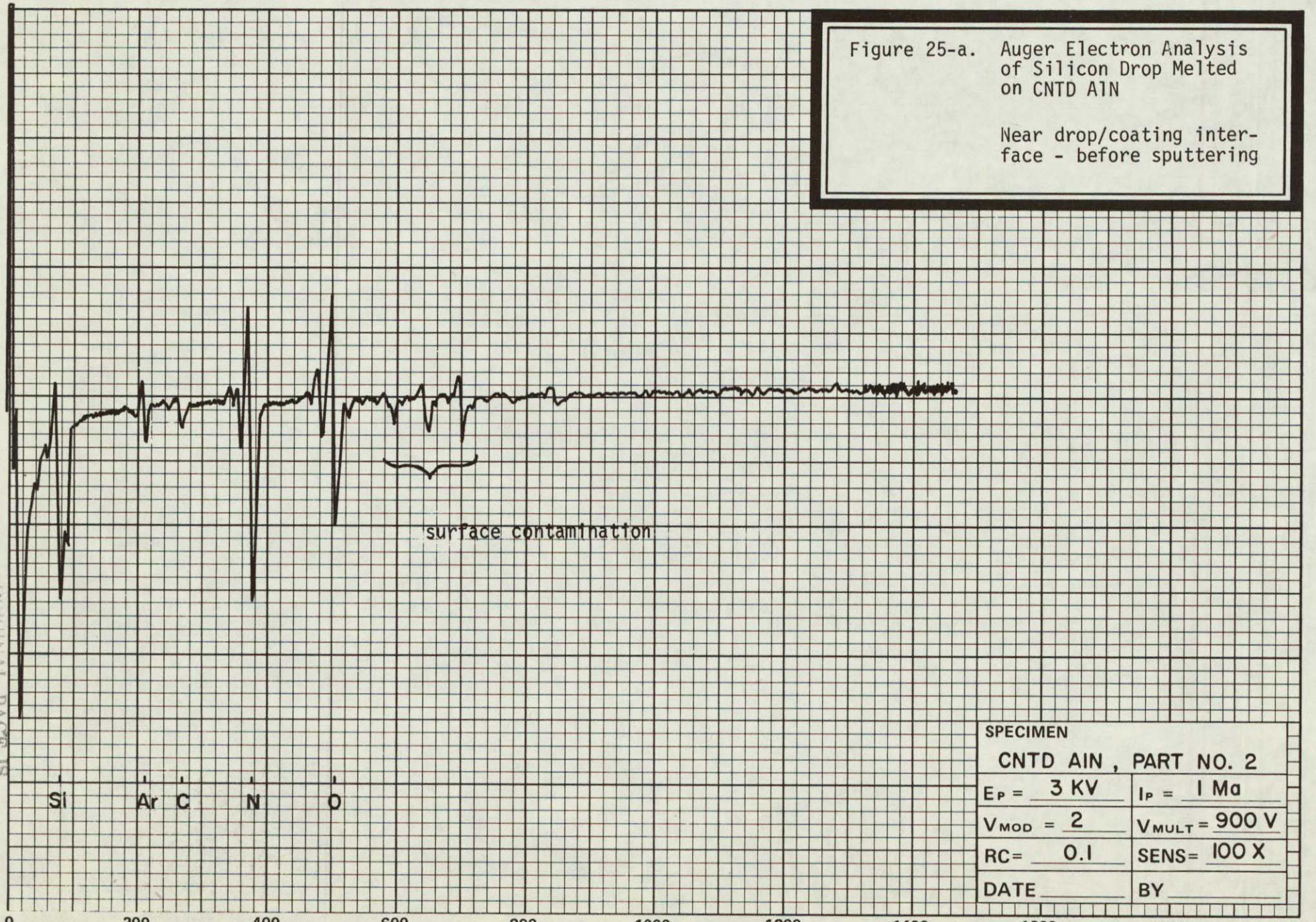

SPECIMEN	
CNTD AIN , PART NO. 2	
E_P = 3 KV	I_P = 1 Ma
V_{MOD} = 2	V_{MULT} = 900 V
RC= 0.1	SENS= 100 X
DATE	BY

PHYSICAL ELECTRONICS INDUSTRIES
AUGER CHART 471022

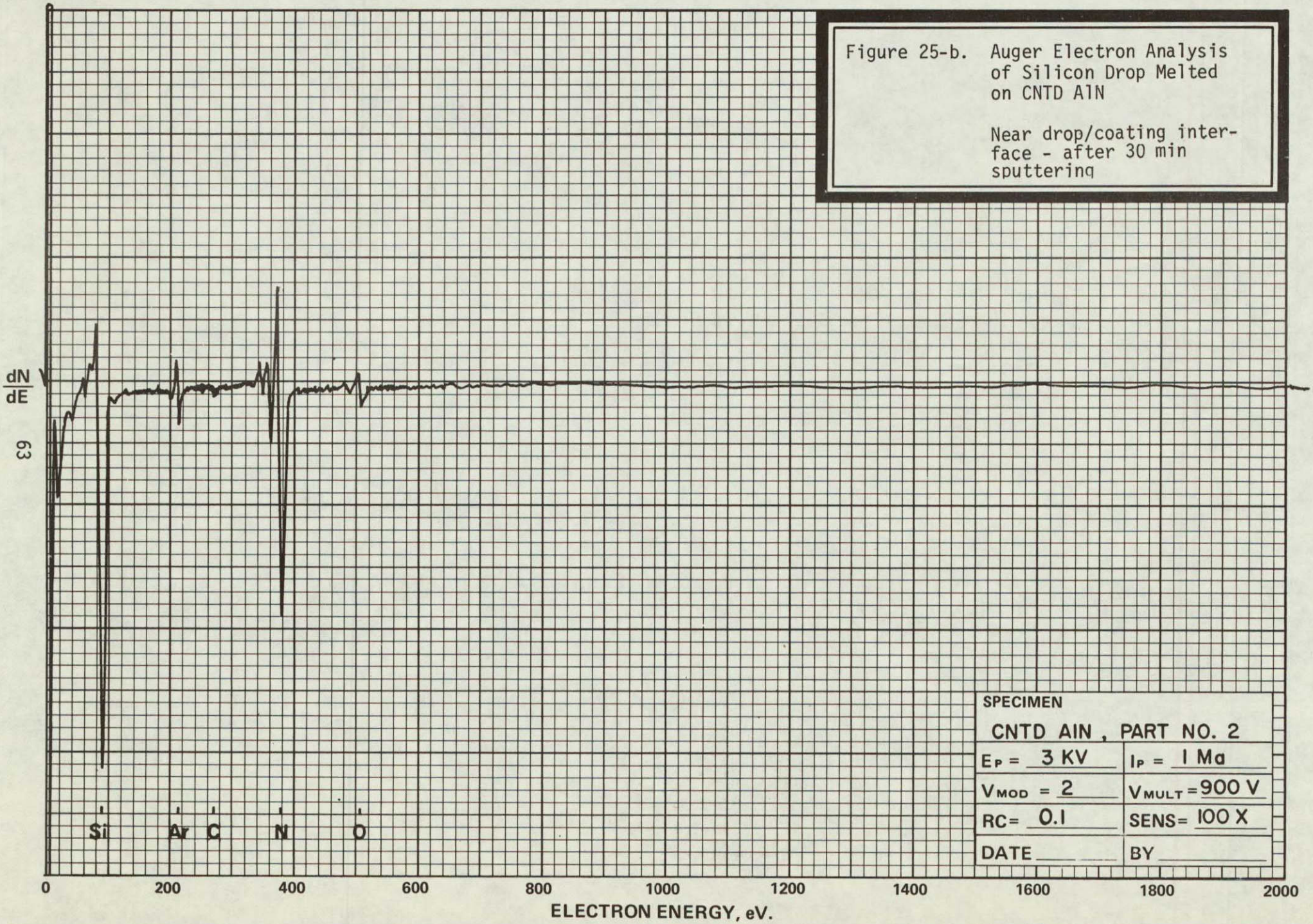

Figure 25-b. Auger Electron Analysis of Silicon Drop Melted on CNTD AlN

Near drop/coating interface - after 30 min sputtering

PHYSICAL ELECTRONICS INDUSTRIES
AUGER CHART 471022

Figure 25-c. Auger Electron Analysis of Silicon Drop Melted on CNTD AlN

Near drop/coating interface - after 87 min. sputtering

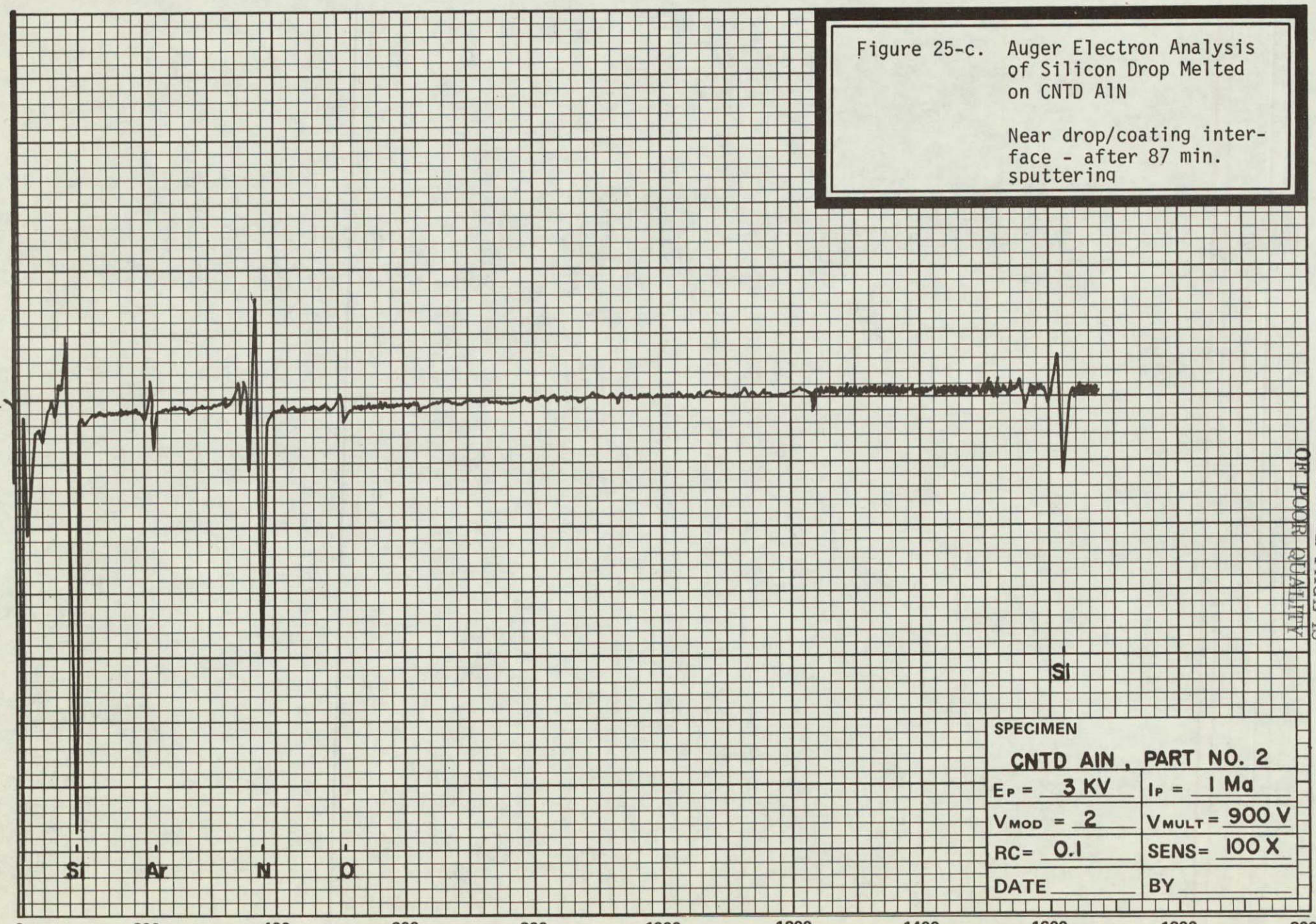

SPECIMEN	
CNTD AIN , PART NO. 2	
E_P = 3 KV	I_P = 1 Ma
V_{MOD} = 2	V_{MULT} = 900 V
RC= 0.1	SENS= 100 X
DATE	BY

sent regions of varying phase content. The latter hypothesis is very difficult to investigate due to the existence of a large number of polytypes of α-SiC. The potential of CNTD fabrication for producing fine grained, crystalline SiC is never-the-less established. No amorphous phases were observed.

The CNTD Si_3N_4 coatings contain small grains (1 μ demonstrated) but appear to contain larger grains also. They may, in addition, be partially or totally amorphous. The altered Si_3N_4 coatings were investigated more extensively due to their expected degree of complexity. The smallest demonstrated grain size was 1 μ, however, the tests are destructive and complete information may not be obtained on a large number of samples until after the sessile drop experiments have progressed further.

The altered Si_3N_4 coatings are indicated by Laue back reflection of a columnated x-ray beam to contain some relatively large grains (up to 600 μ). Scanning electron microscopy verified the existence of large grains in these materials (Figure 10). The effect of grain size on the performance of these materials in contact with molten silicon is not known.

The principal crucible hot pressing problems have been resolved clearing the way for delivery of that hardware item. Die blank fabrication proceeded smoothly and grinding development is underway.

6. PROJECTED ACTIVITIES FOR THE FIFTH QUARTER

6.1 MIAMI RESEARCH LABORATORIES

SiC crucibles will be hot pressed and SiC dies will be hot pressed and ground. Si_3N_4 dies will be ground.

The emphasis in characterization will shift to post sessile drop specimens, however, information concerning the CNTD microstructure will be continued in that work.

6.2 UNIVERSITY OF MISSOURI-ROLLA

Careful sessile drop experiments will proceed in the calibrated apparatus under precisely measured oxygen partial pressures. Test times and temperatures will also be varied. Auger and SEM characterization of the interfaces will continue.

6.3 CHEMETAL

CNTD Si_3N_4 will be applied to hot pressed Si_3N_4 crucibles (PP-30, "impure", w/4 wt% MgO) and to hot pressed and ground Si_3N_4 dies (PP-33, "pure", w/4 wt% MgO). CNTD SiC coatings may be applied to hot pressed SiC crucibles and dies dependent upon fabrication of these articles at the Miami Research Laboratory.

REFERENCES

1. Washburn, Malcolm E., Ceramic Bulletin, Vol. 46, No. 7, pp 667-671, (1967)

2. "A Computed X-Ray Diffraction Pattern for Alpha and Beta Silicon Nitride"; Gazzara, Charles P. and Reed, David; Army Materials and Mechanics Research Center, AMMRC TN 75-4, April (1975).

3. Dr. James E. Thomas, Pittsburg State University, Pittsburg, KS, Personal Communication

4. R. Littlewood, Can. Met. Q.S, 1-17 (1966)

5. R.J. Fruehan and F.D. Richardson, Trans. Metall. Soc. AIME 245, 1721-1726 (1969)

6. A.G. Karaulov, A.A. Grebenjuk, N.V. Gul'ko, I.N. Rudyak, and E.I. Zoz, Ogneupory 45-51 (1968)

7. G.R. Fitterer, J. Metals 18, 961-966 (1966) and J. Metals 19, 92-92 (1967)

8. G.R. Fitterer, C.D. Cassler, and V.L. Vierbicky, J. Metals, 21, 46-52, (1969)

9. M. Matsushita and K. Goto in "Thermodynamics" Int. Atom. Energy Agency, Vol. 1, 111-129, Vienna

10. J.W. Patterson, E.C. Bogren and R.A. Rapp, J. Electrochem. Soc. 114, 752-758 (1967)

APPENDIX

APPENDIX

DETAILED DISCUSSION OF THE X-RAY DIFFRACTION CHARACTERIZATION OF THE ALTERED Si_3N_4 COATINGS (GROUP 4-A and 4-B)

A.1 PEAK IDENTIFICATION

Coating materials 4-A and 4-B were analyzed by x-ray diffraction using Cu Kα radiation from 2Θ equals 0^o to 100^o. However, due to modification of the sample holder for the coated substrates, the low angle beam was totally blocked for 2Θ angles less than 16^o.

Both coating materials and substrates were checked against the ASTM card files for Si_2ON and Y_2O_3. They were also checked for Si_2ON_2 using data obtained from the literature[1] and for α - Si_3N_4 and β - Si_3N_4 using computed powder x-ray diffraction data from an AMMRC report. Only α - Si_3N_4 was detected in the 4-A and 4-B coatings and the Si_3N_4 w/10 wt% Y_2O_3 substrates were β-phase. Several coatings from each lot showed no peaks and were probably amorphous while others showed a higher than normal background indicating the possible presence of some amorphous material. Tables A-I and A-II of the main body list these results. This shows that the hopes of depositing Si_2ON_2 (4-A) and SiAlON (4-B) were not realized.

No unknown peaks were detected for $2\Theta < 60^o$ and no significant unknown peaks were detected at higher angles. One of the variances noted was that all peaks on both the substrates and coatings deviated in 2Θ angle from the computed data of AMMRC. This same effect had been noted on all previous coatings analyzed by x-ray diffraction. The peaks were consistently at a lower angle than expected, with the largest

displacement occurring at low angles with decreasing displacements occurring as the angle increased but never reaching zero displacement. The actual displacement was not consistent from sample to sample and was from 0.2^{o} to 0.7^{o} at low angle ($\approx 30^{o}$) down to 0.1^{o} to 0.3^{o} at the highest angle ($\approx 100^{o}$). A lattice parameter change could possibly cause an angular displacement of the peaks but this displacement would normally be expected to vary in the opposite manner (largest at the higher angles) and was therefore not considered to be a probable explanation of the observed effect. The alignment of the x-ray diffractometer was determined to be well within specification and Si_3N_4 powder, using the standard powder mounting procedure, did not show any angular displacement of the peaks.

In an effort to determine the origin of these displacements, an x-ray diffractometer at Pittsburg State University, Pittsburg, Kansas, was used to run a sample which had shown large angular displacement. After careful alignment of the machine at P.S.U., this sample showed all peaks to be within 0.1^{o} of the values listed by AMMRC. The displacement problem is now considered to be a mechanical alignment problem not associated with the coating and that lattice parameter changes, if present, were not detected.

A.2 RELATIVE INTENSITIES

Two x-ray diffraction scans were made for each coating sample without demounting. The sensitivities of the two scans were adjusted to a ratio of one to five enabling the more intense peaks to remain on scale for intensity measurements while also allowing lower intensity peaks to be detected. Peak intensities could then vary by a factor

of approximately 100 and still be measurable.

As experienced on some of the previous coating materials, the measured relative intensities did not agree with the literature (in this case the AMMRC calculated intensities). The ratios of the observed to expected intensities were estimated to be as much as a factor of 20 in individual cases but were more commonly near 10. The samples of lot 4-A showed some consistency in the particular peaks that were high and low whereas, samples from lot 4-B showed much less consistency. Table A-I lists the AMMRC calculated relative intensities and the experimental intensities for two coatings of lot 4-A and one coating of lot 4-B. Only the calculated relative intensities greater than one are included. The experimental intensities have been normalized so that the sum for one coating is equal to the sum of the calculated intensities. The first two experimental columns are typical of lot 4-A and show several peaks that were consistently high and several that were consistently low. This degree of regularity was not noted in the samples from lot 4-B. It should be noted, however, that the (100) line would not be detectable because of the obstruction of the x-ray beam by the mount and that other low angle lines could have been at least partially affected by this same feature. When three of the specimens (from both lots 4-A & 4-B) were run on the x-ray machine P.S.U., the (100) line was still not detectable and the other low angle lines did not seem significantly different in intensity. In all cases of lot 4-A run at both the Eagle-Picher lab and at P.S.U. the (222) line was the most intense. This, however, was not generally true of those from lot 4-B. Table A-II gives the calculated (from AMMRC)

TABLE A-I

Calculated & Experimental Intensities

		Lot 4-a		Lot 4-b
hkl	Calc.	#4	#5	HP-381A
100	15	0	0	0
101	100	6	3	20
110	48	11	0	1
200	32	6	1	4
201	99	54	38	83
002	11	0	1	19
102	89	9	5	79
210	90	54	1	9
211	66	115	63	26
112	3	6	20	6
300	2	2	0	2
202	38	8	11	36
301	42	44	25	10
220	5	2	0	0
212	8	3	10	6
310	8	8	0	20
103	11	0	0	35
311	17	38	31	12
302	1	*	*	*
203	8	2	1	32
222	22	192	230	140
312	3	11	19	5
320	3	0	0	1
213	5	8	21	11
321	31	27	2	10
410	1	*	*	6
402	1	*	*	*
303	26	7	12	22
411	25	39	7	10
004	14	0	0	20
104	4	0	0	7
322	32	128	140	83
500	1	*	?	*

TABLE A-I
(Continued)

Calculated & Experimental Intensities

313	8	?	?	38
114	5	?	?	?
501	6	8	0	0
412	20	21	10	25
204	4	?	?	?
330	11	8	0	?
420	3	3	0	0
421	6	11	3	6
214	9	3	4	20
502	2	2	1	1
510	2	0	0	1
323	12	69	150	83
511	6	?	0	1
332	2	8	9	8
422	4	15	17	25
413	8	?	?	?
224	1	*	*	1
314	2	0	2	2
512	4	3	0	3
430	3	3	0	2
503	1	*	*	*
431	2	1	0	2
520	1	*	*	*
205	3	0	2	9
521	1	*	*	*
423	4	12	40	12
324	5	11	69	19
610	2	?	0	?
513	5	7	67	6
611	4	4	0	1

? Peak intensity not discernable

* Calculated intensity too low to be detectable at normal experimental intensity

and experimental (run at P.S.U.) ratios of the intensities of the (222) line to the five calculated most intense lines. These are for two specimens (one from lot 4-A and one from lot 4-B) that were run repeatedly at different surface positions and orientations. The experimental ratios are significantly larger than the calculated ratios.

These intensity variations could possibly be explained by an oriented overgrowth, a non-uniformity of crystallite size, a change in the structure factor due to the mechanism of deposition, or non-stoichiometry or any combination of these. Although a complete investigation could not be made, it was suggested[3] that a quick method was available that might provide more insight to the situation.

TABLE A-II

RATIOS OF (222) PEAK INTENSITIES TO FIVE STRONG PEAKS[a]

		X-ray Run #					
Peak Comparison	Calculated[b]	A-1	A-2	A-3	A-5	B-1[d]	B-2
(222)/(101)	22%	>220%	150%	280%	>230%	280%	260%
(222)/(201)	22%	>910%	200%	140%	>380%	115%	180%
(222)/(102)	25%	>1000%	330%	430%	>1100%	1330%	**
(222)/(210)	24%	*	*	*	*	440%	560%
(222)/(211)	33%	>1000%	450%	410%	>590%	310%	320%

* The (210) peak missing or not intense enough to be measurable.

** The (102) peak missing

[a] As measured from patterns run at Pittsburg State University of Pittsburg, Kansas

[b] From the AMMRC report

[c] A-1, A-2, A-3, A-4, A-5 made on coating HP-386A of lot 4-b at various positions and orientations.

[d] B-1 & B-2 made on coating #2 of lot 4-a at different orientations.

A Laue camera, (Figure A-8) normally used to orient single crystals, was used with unfiltered copper radiation. Spots appear on the film when the Bragg condition is met for a given plane and one particular wavelength of the impinging continuous or polychromatic radiation. When a randomly oriented polycrystalline substance is used for the sample, all planes will find a wavelength of radiation that will satisfy the Bragg condition for their particular orientation and the film should show a large number (at least one for every reflecting plane) of randomly oriented spots. However, since there is also a characteristic radiation present (the K_α and K_β lines) that may be more intense (as is the case here) than the continuous radiation, the spots due to the characteristic radiation will be clustered in circular rings. These would be from those planes having the proper orientation and d-spacing to meet the Bragg condition for the $Cu_{k\alpha}$ or K_β wavelength. If the incident x-ray beam is columnated and is larger than the largest crystallite, the spots from both the characteristic and continuous radiation will be approximately the same size and shape as the reflecting planes. If the specimen is not composed of randomly oriented crystallites then the spots will show a lack of randomness and the characteristic radiation rings will not be equally populated in all circumferential locations.

Three samples from lot 4-A have been studied using this method. Spot sizes, and thus crystallite sizes, (beam divergence and camera geometry accounted for) have been detected from $\tilde{\sim}$ 0.1 mm to 0.6 mm in diameter. Some of these showed shape features. These sizes cannot be viewed as inclusive because only those planes meeting the Bragg

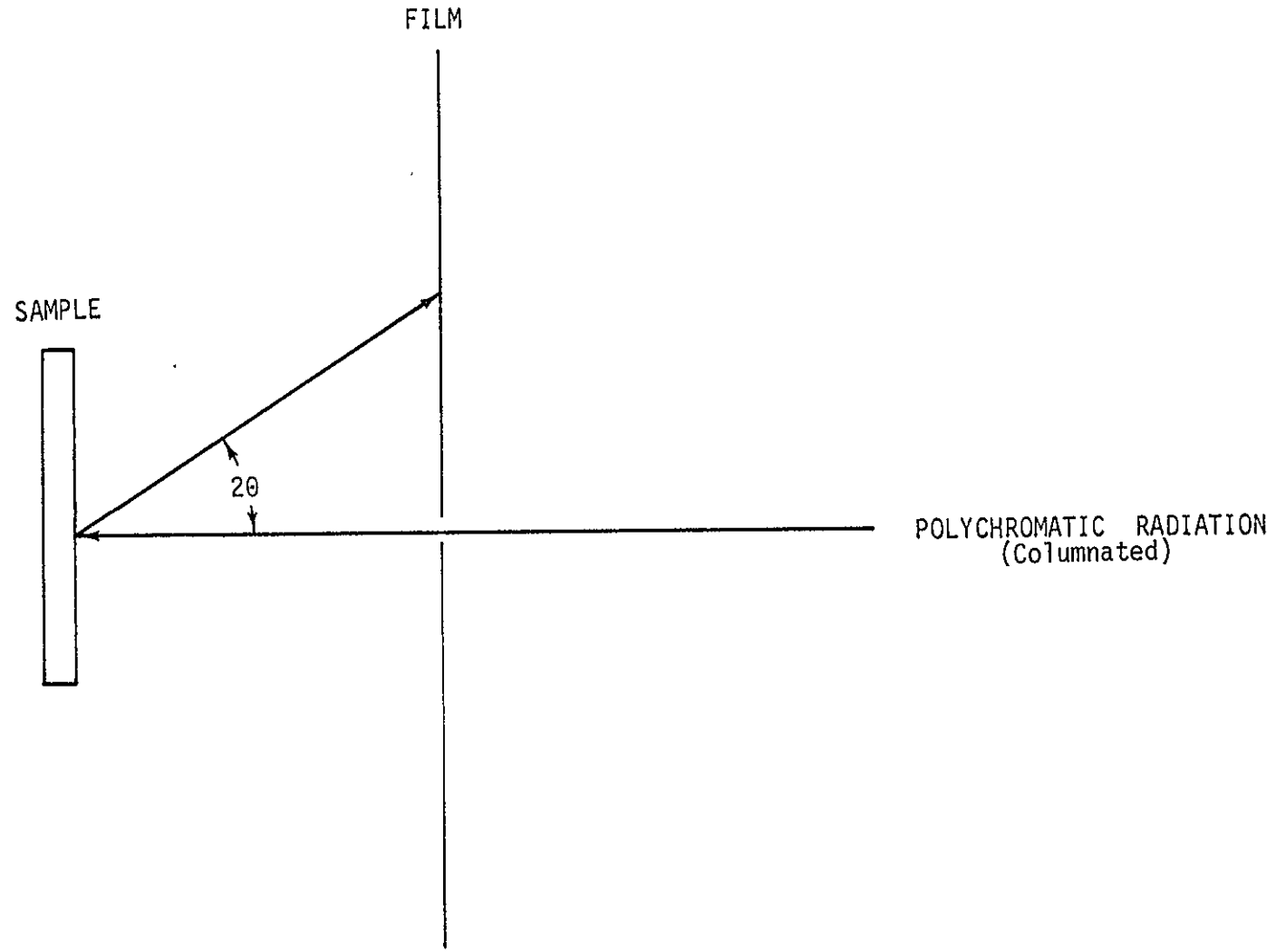

Figure A-8. Laue Camera Experimental Set-up for Investigating Possible Orientation in the Coatings

condition were seen and this is only a fraction of the total. Also, sizes smaller than 0.1 mm were not detectable by this procedure.

The samples have been run at various positions on the surface and at various orientations with respect to the incident beam in an effort to find a positive indication of preferred orientation of the coatings. The results indicate that the orientation, if present, is very slight and not of the degree necessary to explain the large deviations in peak intensities. In one sample it was found that the larger crystallites did have some (probably small) degree of orientation since they seemed to be more densely populated on one portion of the characteristic circular ring than at others. This was true over the face of the coating. However, the direction at which the more densely populated portion existed varied as the incident beam was moved to different spots on the surface.

All of this indicates that, although preferred orientation can still not be ruled out, there has been no indication of a strong degree of orientation. The crystallite sizes did vary considerably and the larger crystallites could be locally oriented but no long range orientation was detected for them either. The possibility of a change in structure factor was not investigated since the only method available was to grind the coating off and x-ray it as a powder.